ROBUST SIGMOIDAL COST FRAMEWORK BASED LMS ALGORITHMS FOR SHUNT COMPENSATION IN GRID-CONNECTED SYSTEM

DISSERTATION / THESIS

SUBMITTED IN PARTIAL FULFILMENT OF THE REQUIREMENTS
FOR THE AWARD OF THE DEGREE
OF

MASTER OF TECHNOLOGY
IN
POWER SYSTEMS

Submitted by:

Neeraj Singh Bisht

Roll No. 2K20/PSY/14

Under the supervision of:

Ankita Arora

Assistant Professor

DEPARTMENT OF ELECTRICAL ENGINEERING
DELHI TECHNOLOGICAL UNIVERSITY
(Formerly Delhi College of Engineering)
Bawana Road, Delhi – 110042

May, 2022

DEPARTMENT OF ELECTRICAL ENGINEERING
DELHI TECHNOLOGICAL UNIVERSITY
(Formerly Delhi College of Engineering)
Bawana Road, Delhi-110042

CANDIDATE'S DECLARATION

I, Neeraj Singh Bisht, Roll No. 2K20/PSY/14, student of M.Tech. (Power System), hereby declare that the project Dissertation titled "Robust Sigmoidal Cost Framework Based LMS Algorithms for Shunt Compensation in Grid-Connected System" which is submitted by me to the Department of Electrical Engineering Department, Delhi Technological University, Delhi in partial fulfilment of the requirement for the award of the degree of Master of Technology, is original and not copied from any source without proper citation. This work has not previously formed the basis for the award of any Degree, Diploma, Associateship, Fellowship or other similar title or recognition.

Place: Delhi — Neeraj Singh Bisht
Date: — 2K20/PSY/14

DEPARTMENT OF ELECTRICAL ENGINEERING
DELHI TECHNOLOGICAL UNIVERSITY
(Formerly Delhi College of Engineering)
Bawana Road, Delhi-110042

CERTIFICATE

I hereby certify that the project dissertation/thesis titled "Robust Sigmoidal Cost Framework Based LMS Algorithms for Shunt Compensation in Grid-Connected System" which is submitted by Neeraj Singh Bisht, Roll No. 2K20/PSY/14, student of Department of Electrical Engineering, Delhi Technological University, Delhi in partial fulfilment of the requirement for the award of the degree of Master of Technology, is a record of the project work carried out by the student under my supervision. To the best of my knowledge this work has not been submitted in part or full for any Degree or Diploma to this university or elsewhere.

Place: Delhi
Date:

Ms. Ankita Arora
SUPERVISOR
Assistant Professor
Department of Electrical Engineering
Delhi Technological University
Bawana Road, Delhi-110042

ABSTRACT

In recent times AC grid connected systems are experiencing numerous power quality problems mostly originating in distribution level. Use of power converter-based machines in industries, homes, shops, offices, and traction applications have seen an exponential increase. These equipment behave as nonlinear load, draw non-sinusoidal current and cause Power Quality deterioration of supply system. In this work power quality issues due to increased application of renewable energy resources and non-linear loads and in distribution system are addressed. There are a number of current-based power quality problems such as poor voltage regulation, poor power factor, harmonics distortion, unbalanced currents etc. DSTATCOM are becoming more applicable for improving the condition of power quality in supply systems due to cost benefits. Due to increase in computational capacities of modern computers adaptive filters are becoming popular in wide areas of noise/echo cancellation, adaptive control, image restoration and channel equalization. DSTATCOM with adaptive filtering technique are being used as a cost-effective Shunt Active Power Filter (SAPF). Most simple control strategies based on adaptive filter, for SAPF, are the Least Mean Square (LMS) algorithm and its versions, because of their simplicity and relatively robust performance. Various issues such as performance degradation in presence of outlier conditions like impulsive current and voltage variations which commonly happens during practical system operation. Several LMS-Adaline based Control Algorithms of DSTATCOMs have been implemented in various articles. In this project the aim is to implement a more robust LMS based algorithm for DSTATCOM control using sigmoid cost-framework, which reduces performance degradation due to impulsive interferences. Using sigmoid cost framework

sigmoidal least absolute difference (SLAD), sigmoidal least logarithmic absolute difference (SLLAD), sigmoidal least mean square (SLMS), sigmoidal least mean logarithmic square (SLMLS) and sigmoidal least mean fourth (SLMF) algorithms for DSTATCOM control are simulated in MATLAB/Simulink environment. A comparison between various algorithms is presented. A PV-DSTATCOM for PV-grid integration, using SLMLS algorithm and Maximum Power Point Tracking (MPPT) algorithm using incremental conductance method, is also simulated and results are analysed.

ACKNOWLEDGEMENT

I am highly grateful to the Department of Electrical Engineering, Delhi Technological University (DTU) for giving me the opportunity to carry out this project work. The constant guidance and encouragement received from my supervisor Ms. Ankita Arora of Department of Electrical Engineering, DTU, has been of great help in carrying my present work. I would also like to thank Prof Suman Bhowmick, Prof Alka Singh and Prof S T Nagarajan for their reviews and comments that helped in improving the quality of this work. Finally, I would like to express my gratitude to the faculty members of Electrical Engineering Department, DTU for their continuous support in my M. Tech. study at DTU. I would like to thank my brother Mr. Pushkar Singh Bisht for sponsoring my master's study.

Neeraj Singh Bisht
2K20/PSY/14
M. Tech. (Power Systems)
Delhi Technological University

CONTENTS

Candidate's Declaration ii

Certificate iii

Abstract iv

Acknowledgement vi

Contents vii

List of Tables xi

List of Figures xii

CHAPTR 1 INTRODUCTION: POWER QUALITY STANDARDS AND CONTROL 1

1.1 Power Quality Problems 1

1.1.1 Classification of Power Quality Problems 2

1.1.2 Effects of Power Quality Problems 3

1.2 Standards for Power Quality 4

1.3 Techniques for Mitigating Power Quality Problems 6

1.3.1 Mitigation of Transient Problems 6

1.3.2 Frequency Control 6

1.3.3 Voltage Control 7

1.3.4 Control of Waveform Distortion 8

1.4 Introduction to MATLAB/Simulink 9

1.5 Outline of The Thesis 10

CHAPTER 2 LITERATURE SURVEY: STATIC SYNCHRONOUS COMPENSATOR FOR POWER QUALITY IMPROVEMENT 12

2.1 Operation of STATCOM 12

2.2 STATCOM V-I Characteristic 14

2.3 Circuit Configurations of Shunt Connected STATCOM 16

2.4 Applications of Shunt Connected STATCOM 17

2.4.1 Mid-Point Voltage Regulation 18

2.4.2 End-Point Voltage Stability Improvement 18

2.4.3 Transient Stability Improvement 19

2.4.4 Damping Power Oscillations 19

2.4.5 STATCOM for PV-Grid Integration 20

2.4.6 STATCOM as Shunt Active Power Filter 20

2.5 Control of STATCOM as Shunt Active Power Filter 20

2.5.1 LMS Based Adaline Algorithm 22

2.6 PV-Grid Integration 26

2.7 Objectives of Current Work 26

2.8 Chapter Summary 27

CHAPTER 3 DSTATCOM CONTROL FOR POWER QUALITY IMPROVEMENT WITH SIGMOID BASED ALGORITHMS 28

3.1 Sigmoid Cost Framework Based Algorithms 28

3.1.1 Sigmoid Least Mean Square (SLMS) Algorithm 28

3.1.2 Sigmoid Least Absolute Difference (SLAD) Algorithm 29

3.1.3 Sigmoid Least Mean Fourth (SLMF) Algorithm 29

3.1.4 Sigmoid Least Logarithmic Absolute Difference (SLLAD) Algorithm 30

3.1.5 Sigmoid Least Mean Logarithmic Square (SLMLS) Algorithm 30

3.2 Design and Implementation of Three Phase Distribution System with DSTATCOM 30

3.2.1 Design and Modelling of Supply and Loads 31

3.2.2 Design and Modelling of DSTATCOM 32

3.3 Implementation of DSTATCOM Control Algorithms 33

3.3.1 Unit Vector Generation Block 33

3.3.2 Block for Generating Reference Current 34

3.3.3 Hysteresis Current Controller 35

3.3.4 Weight Estimation Blocks for Different Algorithms 35

3.4 Simulation Results and Discussion 39

3.4.1 Results for Adaline-LMS Algorithm 39

3.4.2 Results for SLMS Algorithm 40

3.4.3 Results for SLAD Algorithm 40

3.4.4 Results for SLMF Algorithm 41

3.4.5 Results for SLLAD Algorithm 41

3.4.6 Results for SLMLS Algorithm 42

3.4.7 Comparison Between Adaline-LMS and Sigmoid Algorithms 42

3.4.8 Comparison Between Sigmoid Based Algorithms 44

3.5 Chapter Summary 46

CHAPTER 4 DSTATCOM CONTROL FOR PV-GRID INTEGRATION 47

4.1 Characteristics of PV Modules 47

4.2 System Design and MATLAB Modelling 49

4.2.1 Design and Implementation of PV System 50

4.2.2 Boost Converter Design and Implementation 51

4.3 Controlling the PV-DSTATCOM System 52

4.3.1 Method of Incremental Conductance 52

4.3.2 DSTATCOM Control with SLMLS Algorithm 53

4.4 Simulation Results and Discussion 54

4.4.1 Performance of DSTATCOM 55

4.4.2 Performance of Incremental Conductance Algorithm 57

4.5 Chapter Summary 59

CHAPTER 5 CONCLUSIONS AND FUTURE SCOPE 60

REFERENCES 62

LIST OF PUBLICATIONS 66

LIST OF TABLES

Table 1.1 Distortion limits for voltage 5

Table 1.2 Distortion limits of current for system's voltage rated above 161 kV 5

Table 1.3 Distortion limits of current for system's voltage rated 69 kV to 161 kV 5

Table 1.4 Distortion limits of current for system's voltage rated 120 V to 69 kV 5

Table 3.1 Percentage THD (% of fundamental at 50 Hz) in source voltage and current 44

LIST OF FIGURES

Fig. 2.1 STATCOM connected to utility bus 13

Fig. 2.2 Operation of VSC 14

Fig. 2.3 STATCOM V-I characteristics 15

Fig. 2.4 Operation of STATCOM 15

Fig. 2.5 Single phase half bridge STATCOM circuit configuration 16

Fig. 2.6 Single phase full bridge STATCOM circuit configuration 16

Fig. 2.7 Three-leg three-wire STATCOM configuration 17

Fig. 2.8 Three H-bridge four-wire STATCOM configuration 17

Fig. 2.9 STATCOM mid-point compensation and phasor diagram 18

Fig. 2.10 STATCOM for load end voltage stability 18

Fig. 2.11 Power versus transmission angle curve 19

Fig. 2.13 General block diagram of adaptive filter 22

Fig. 2.14 Three phase three-wire DSTATCOM system 23

Fig. 2.15 Generalised block diagram representation of LMS algorithm 25

Fig. 3.1 Circuit diagram of proposed system 31

Fig. 3.2 MATLAB implementation of system 32

Fig. 3.3 MATLAB implementation of unit vector generation block 34

Fig. 3.4 MATLAB implementation of reference current generation block 34

Fig. 3.5 MATLAB implementation of hysteresis current controller 35

Fig. 3.6 MATLAB implementation of weight estimation for LMS-Adaline algorithm 35

Fig. 3.7 MATLAB implementation of weight estimation for SLMS algorithm 36

Fig. 3.8 MATLAB implementation of weight estimation for SLAD algorithm 36

Fig. 3.9 MATLAB implementation of weight estimation for SLMF algorithm 37

Fig. 3.10 MATLAB implementation of weight estimation for SLLAD algorithm 37

Fig. 3.11 MATLAB implementation of weight estimation for SLMLS algorithm 38

Fig. 3.12 MATLAB implementation of control algorithm 38

Fig. 3.13 Results for Adaline-LMS algorithm 39

Fig. 3.15 Results for SLMS algorithm 40

Fig. 3.16 Results for SLAD algorithm 40

Fig. 3.17 Results for SLMF algorithm 41

Fig. 3.18 Results for SLLAD algorithm 41

Fig. 3.19 Results for SLMLS algorithm 42

Fig. 3.19 Weight update comparison of Adaline-LMS and SLMS algorithm 43

Fig. 3.20 DC bus voltage comparison of Adaline-LMS and SLMS algorithm 43

Fig. 3.21 Comparison of Adaline-LMS and SLMS algorithms for impulsive load 44

Fig. 3.22 Weight update comparison for sigmoid based algorithms 45

Fig. 3.23 DC bus voltage comparison for sigmoid based algorithms 46

Fig. 4.1 P-V and I-V curve for different irradiance levels of PV 48

Fig. 4.2 P-V and I-V curve for different temperature levels of PV 48

Fig. 4.3 STATCOM for PV-Grid integration 49

Fig. 4.4 Equivalent circuit representation of PV array 51

Fig. 4.5 P-V and I-V characteristics of PV array at 25 °C 51

Fig. 4.6 MATLAB implementation of incremental conductance algorithm 54

Fig. 4.7 DSTATCOM control for PV integrated system 54

Fig. 4.8 Results for PV integrated system 55

Fig. 4.9 Source current’s harmonic spectra at 0.05 seconds 56

Fig. 4.10 Source current’s harmonic spectra at 0.15 seconds 56

Fig. 4.11 Source current’s harmonic spectra at 0.4 seconds 57

Fig. 4.12 Source current’s harmonic spectra at 0.7 seconds 57

Fig. 4.13 Source current’s harmonic spectra at 0.9 seconds 58

Fig. 4.14 PV array terminal current and voltage 58

Fig. 4.15 Instantaneous reactive and active power 59

CHAPTER 1

INTRODUCTION:
POWER QUALITY STANDARDS AND CONTROL

The term Power Quality can be defined in many ways based on systems and their applications. It can be referred to as the ability of efficiently utilizing the power supplied by a system to electrical equipment. According to the IEEE dictionary the power quality definition is stated as: “Power quality is the concept of powering and grounding sensitive equipment in a manner that is suitable to the operation of that equipment.” Thus, an electrical equipment designed to work on DC supply can not be given AC supply as input and suitable means of power conversion have to be used. In AC systems equipment designed to work at 60 Hz frequency of supply like in US and UK will suffer malfunction or failure if used with 50 Hz supply used in India.

The term power quality as defined by IEC in IEC 61000-4-30, states “Characteristics of the electricity at a given point on an electrical system, evaluated against a set of reference technical parameters.” Thus, Power Quality can be defined as a set of boundaries within which electrical system performs the task efficiently for which it is designed. These boundaries are defined in percentage of the voltage, frequency and waveform deviations of a power supply system. These boundaries help manufacturers design and manufacture equipment based on uniform standards which reduces the cost and the equipment can be used at any geographic location without any performance issues.

1.1 POWER QUALITY PROBLEMS

Power Quality problems like poor power factor, voltage fluctuations, waveform distortions etc have been present in electrical power system since the

beginning. These problems are caused by faults, motor loads, lightening, equipment malfunction etc. Equipment like circuit breakers, lightening arrestors, motor starters, synchronous condensers etc are designed to mitigate or override their effect on the power system. In present scenario, with increased interconnectivity between traditional sources for reliability of supply and induction of power electronic converter based renewable energy sources, the sensitivity of the system has increased exponentially. On the consumer side the use of power electronic converter-based devices, such as battery chargers, Adjustable Speed Drives (ASDs), furnaces, Uninterruptible Power Supplies (UPSs) etc, cause waveform distortions and frequency deviations as they draw non-sinusoidal current and their behaviour is characterized as nonlinear loads. The use of these solid state-based devices has many benefits such as reduced size, maintenance requirements and cost; increased efficiency and better control.

1.1.1 CLASSIFICATION OF POWER QUALITY PROBLEMS

Classification of Power Quality problems can be done in many ways such as cause of occurrence, location of occurrence, based on quantity under consideration, duration of event etc. Based on cause these problems are classified as natural and man-made. Problems due to natural causes such as lightening, faults etc are over voltages, transients, distortions etc. Man-made problems include harmonic currents caused by nolinear loads, reactive power requirement etc.

Based on duration of the event Power Quality issue can be transient in nature or Steady-State type. In transient type includes impulsive voltage or current for very short duration, such as sag in voltage (dip), swell, voltage transients, short-term frequency deviations etc. The steady-state type includes long-term voltage deviations, unbalanced currents, notches, flicker, waveform distortions, DC-offset, low power factor etc.

On the basis of quantity being affected Power Quality issues can be concerned with voltage, current or frequency. Problems related to voltage include waveform distortions, sag, notches, flicker, swell, unbalance, DC offset; problems related to current are excessive reactive power, harmonics, unbalanced in three-phase currents and excessive current through neutral. Frequency variations can cause malfunction, losses, inaccuracy or damage to sensitive equipment.

Based on the location Power Quality problems may be in load, supply system or transmission system. Due to nature of the load issues like harmonics in current and voltage, requirement of reactive power, unbalanced three-phase currents, excessive current in neutral and DC-offset arise. The power quality issues arising in the generation system related to voltage and frequency are due to loss of synchronism, over or under excitation. In transmission system faults and line capacitance and inductance cause variations in voltage, reactive power requirement, noise etc.

1.1.2 EFFECTS OF POWER QUALITY PROBLEMS

Power Quality issues concern all the stakeholders (Generation units, transmission units and consumers) in a power system network. Interruption of power supply due to Power Quality problems causes revenue losses to commercial and industrial consumers as it results in loss of important data, production loss, interruption of process, wastage of raw material etc. Sensitive consumer equipment may malfunction or get damage due to voltage fluctuations, frequency deviations, harmonics, overcurrent or overvoltage. Poor power factor and harmonics cause increased losses in the machines which increases cost of operation and reduces life of equipment.

In transmission system Power Quality problems affect the operation of machines, protective devices and measuring instruments. Harmonic currents and frequency deviations increase losses, noise and vibrations in transformer and capacitor bank causing reduced efficiency and increased maintenance cost. Overcurrent and overvoltage due to faults and lightening results in derating of cables, false metering, damage to substation equipment, interference with communication signals, breaker and relay malfunctions.

In conventional generation system requirement of reactive power, unbalanced loads cause voltage instability, loss of synchronism, frequency deviations, excessive neutral currents etc. These problems increase running as well as maintenance costs due to losses and damage to machines. In renewable energy generation such as solar PV cells the produced power is in DC while conventional grid equipment works on AC. Power electronic converters and filter circuits are required to convert power in required form. These converter and filter circuits are highly sensitive to disturbances in the system.

1.2 STANDARDS FOR POWER QUALITY

Power Quality standards are limits of various quantities such as voltage level, waveform distortion, frequency range etc. under which power system operates normally and efficiently. At present several standards are developed related to numerous power quality issues by different countries. Several organizations namely Institute of Electrical and Electronics Engineers (IEEE), International Electrotechnical Commission (IEC), American National Standards Institute (ANSI), European Norms (EN), Computer Business Equipment Manufacturers Association (CBEMA), British Standards (BS), and Information Technology Industry Council (ITIC) have proposed acceptable ranges of various quantities for maintaining Power Quality that sets guidelines for equipment designers, consumers and electrical companies on handling numerous problems that cause Power Quality issues.

Voltage and frequency standards at distribution, transmission and generation are different in different countries. Domestic consumers in India receive electricity at 50 Hz, 230 V while in United States of America the standard is 60 Hz, 110 V. According to Indian Standards (IS)/IEC 60071-1: Insulation Coordination – Definitions, principles and rules, voltage levels are defined as high voltage range II (above 245 kV), high voltage range I (between 1 kV and 245 kV) and low voltage (below 1 kV). While According to ANSI C84.1-1989: "American National Standard for Electrical Power System and Equipment" – Voltage Ratings at 60 Hz are high voltage (between 115 kV and 230 kV), medium voltage (between 2.4 kV and 69 kV) and low voltage (between 120 V and 600 V). In India Indian Electricity Grid Code (IEGC) notified the allowed frequency deviations range as 49.5 to 50.2 Hz and voltage variations of ± 10 % (approx.) from nominal value are permissible.

The IEEE 519-2014 standard: "IEEE Recommended Practice and Requirements for Harmonic Control in Electric Power Systems" [6] prescribes limit of current and voltage waveform variation using percentage harmonic distortion (% of fundamental at 50 Hz or 60 Hz). Table 1.1 gives limits of allowable distortion in voltage at different levels. Table 1.2 shows current distortion limits for system rated above 161 kV. Table 1.3 shows limits of distortion in current for system between 69 kV and 161 kV.

Table 1.4 shows limits of distortion in current for system nominally rated between 120 V and 69 kV.

Table 1.1: distortion limits for voltage

PCC voltage of Bus	V ≤ 1 kV	1 kV ≤ V ≤ 69 kV	69 kV ≤ V ≤ 161 kV	V > 161 kV
Individual harmonics (%)	5.0	3.0	1.5	1.0
Total Harmonic Distortion THD (%)	8.0	5.0	2.5	1.5

Table 1.2: Distortion limits of current for system's voltage rated above 161 kV

Maximum harmonic current distortion in percent of I_L						
I_{SC}/I_L	Individual harmonic order (Odd harmonics)					TDD
	3 ≤ h < 11	11 ≤ h < 17	17 ≤ h < 23	23 ≤ h < 35	35 ≤ h < 50	
< 25	1.0	0.5	0.38	0.15	0.1	1.5
25 to 50	2.0	1.0	0.75	0.3	0.15	2.5
> 50	3.0	1.5	1.15	0.45	0.22	3.75

Table 1.3: Distortion limits of current for system's voltage rated 69 kV to 161 kV

Maximum harmonic current distortion in percent of I_L						
I_{SC}/I_L	Individual harmonic order (Odd harmonics)					TDD
	3 ≤ h < 11	11 ≤ h < 17	17 ≤ h < 23	23 ≤ h < 35	35 ≤ h < 50	
< 20	2.0	1.0	0.75	0.3	0.15	2.5
20 to 50	3.5	1.75	1.25	0.5	0.25	4.0
50 to 100	5.0	2.25	2.0	0.75	0.35	6.0
100 to 1000	6.0	2.75	2.5	1.0	0.5	7.5
> 1000	7.5	3.5	3.0	1.25	0.7	10.0

Table 1.4: Distortion limits of current for system's voltage rated 120 V to 69 kV

Maximum harmonic current distortion in percent of I_L						
I_{SC}/I_L	Individual harmonic order (Odd harmonics)					TDD
	3 ≤ h < 11	11 ≤ h < 17	17 ≤ h < 23	23 ≤ h < 35	35 ≤ h < 50	
< 20	4.0	2.0	1.5	0.6	0.3	5.0
20 to 50	7.0	3.5	2.5	1.0	0.5	8.0
50 to 100	10.0	4.5	4.0	1.5	0.7	12.0
100 to 1000	12.0	5.5	5.0	2.0	1.0	13.0
> 1000	15.0	7.0	6.0	2.5	1.4	20.0

I_{SC} = Maximum short circuit current at PCC.
I_L = Load current (fundamental frequency component) at the PCC under normal load condition
TDD = The RMS value of individual harmonic's, including harmonics of order up to 50 and neglecting interharmonics, as a percentage of the maximum demand current.

1.3 TECHNIQUES FOR MITIGATING POWER QUALITY PROBLEMS

Due to increasing complexity and sensitivity of modern grid because of increasing number of distributed energy generation units, research in the area of Power Quality is drawing interest of engineers primarily those, working in electrical distribution and utilization utilities. Electricity suppliers must ensure that customers receive good quality of power for satisfactory operation of their equipment, and manufacturers need to design their products either to be able to withstand electrical power quality problems or to overcome them. Several methods and devices are already present for maintaining Power Quality in supply, transmission and distribution systems.

1.3.1 MITIGATION OF TRANSIENT PROBLEMS

There are a number of equipment and protection schemes available to mitigate transient Power Quality problems such as overvoltage, overcurrent, disruption of supply and distortions due to lightening, faults, equipment failure, flashover etc. Lightening or surge arrestors are used in substations to divert over-voltages to ground to protect substation equipment. A complex transmission system is divided into protective zones. Primary protection as well as backup protection relays and circuit-breakers are used in each zone to prevent the effect of fault in one zone on entire power system and to ensure reliability of supply.

1.3.2 FREQUENCY CONTROL

A constant frequency and voltage are important factors for good quality of power supply system. Frequency changes affects the speed of synchronous and induction motors. A significant reduction in frequency result in increased magnetising current in induction motors and transformers. The frequency of system depends on balance of active power. In an interconnected system many generator supply power into the system and an active power demand change is reflected as a deviation in frequency throughout the grid. Load-frequency control (LFC) methods are used to ensure regulation of frequency of the power system. Speed governor systems are used as primary control for regulating frequency. When there is a load change the speed-governor changes the turbine output to change the frequency back to its nominal value. A supplementary control is required, in case of interconnection of independently controlled areas, which allocates generation

within each area to maintain scheduled power exchange. Load shedding is a common practice for maintaining frequency within permissible range when frequency drops significantly below the nominal value.

1.3.3 VOLTAGE CONTROL

The voltage in electrical power system is regulated by generation, flow and absorption of reactive power at all stages of the system. As in a grid system power is supplies to a variety of loads and generated using different generating stations, maintaining voltages at nominal values is a challenging task. At the point of generation synchronous generators either consume or supply reactive power based on the level of excitation. Automatic voltage regulators (AVRs) maintains constant voltage at the terminal of generators by controlling field excitation. In solar plants power electronic based power conversion devices are used to maintain nominal voltage at the output.

In transmission system overhead lines either absorb or deliver reactive power depending on its surge impedance and connected load at the end. If the load connected at the end is greater than surge impedance of line, the line absorbs reactive power and voltage of the load side terminals is below the value of voltage of the sending end terminal. If the load connected at the end is lower than surge impedance of line, the line generates reactive power and voltage of the load side terminal is higher than the value of voltage of the sending end terminal. Underground cables have high internal capacitance resulting in high surge impedance and their loading is lower than their surge impedance hence generating reactive power. Transformers always absorb reactive power. Different devices are used to control flow of reactive power in the system.

For long Extra High Voltage (EHV) lines of more than 200 km shunt reactors are employed to avoid ‘Ferranti’ effect due to capacitive line charging current in case of open circuit at the receiving end. Shunt reactors also limit energisation overvoltage and switching transients. Shunt connected capacitor supply reactive power and boost voltage, distributed throughout the length of the line. In distribution systems they are used for control of feeder voltage and correction of power factor.

Series capacitors are used with loads with poor power factor such as arc furnaces and welding machines for voltage regulation and improving power factor. In transmission system series capacitors are used for improving stability of system and power flow control in parallel lines. Synchronous condensers are also used for regulating voltage and control of reactive power. A synchronous condenser is prime mover less synchronous machine with controllable field excitation to adjust reactive power output. As the initial and running cost of synchronous condensers are high they have been replaced by Static Var-Compensators (SVC). SVC is a power electronic based Flexible AC Transmission System (FACTS) device used for regulating voltage, power factor, harmonics and stabilising the system. Thyristor Switched Capacitor (TSC) and Thyristor Controlled Reactor (TCR) are two basic type of reactive power control devices. They are used alone or in different combinations to regulate flow of reactive power in the system. The advantages of using SVCs include lower cost, reduced losses, fast and dynamic control.

1.3.4 CONTROL OF WAVEFORM DISTORTION

Several equipment in the power system draw current in different wave shape than the standard sine wave. These types of equipment are called non-linear loads. The waveform distortion resulting from the operation of these devices affects the working of other equipment of consumers as well as equipment used by utility for measurement, transmission, control and protection. Therefore, it is important that waveform distortion at different levels of the system is within limits. With increased uses of power electronic based converter circuits in consumer products and renewable energy conversion limiting the waveform distortion caused by these equipment is an active area of research. Various types of filters are already in use and new technologies are being developed to lower waveform distortion effects on the system.

Passive shunt filters which consist of either capacitor or inductor or a combination of both are connected in shunt with the non-linear load for giving low impedance path for tuned harmonic frequency components allowing them to pass through passive filter. A simple lossless parallel LC circuit that provide high impedance for blocking harmonic currents act as passive series filter, connected in series with harmonic producing load to prevent harmonic current to enter supply system. These are singly tuned

filters to block dominant third harmonic component. Combination of shunt and series passive filter (Hybrid) are used in many industrial applications. A single tuned passive shunt with a single tuned passive series filter and high pass passive shunt filter gives satisfactory filtering characteristic.

With increasing pollution in AC systems, because of non-linear loads and increased use of power converters, passive filters are becoming inadequate for satisfactory and dynamic filtering of harmonics due to fixed compensation and problems like resonance. To overcome the problem of fixed compensation and dynamic control various active power filters are being used around the world. Series type of active power filter are used to reduce voltage harmonic and imbalance in three phase voltages. Shunt Active Power Filter (SAPF) are shunt connected active filters widely utilised for reducing harmonics, reactive power control, power factor improvement and balancing of load currents. Shunt active power filter with passive shunt filter provide satisfactory and cost-effective solution for dynamic compensation. Various Custom Power Devices (CPDs) namely Unified Power Quality Conditioners (UPQCs), Dynamic Voltage Restorers (DVRs) and Static Synchronous Compensators (STATCOMs) are used for active compensation.

1.4 INTRODUCTION TO MATLAB/SIMULINK

Matrix-Laboratory (MATLAB) is a matrix based high level language which integrates numeric computation, programming and graphic interface for an easy-to-use research and development environment. The MATLAB language represents computing and mathematics is a natural way. With number of Built-in graphical tools data can be easily represented in visual formats for easy understanding and to draw inferences from the data. The easy to use graphical interface aids in quick implementation, editing and makes repeating tasks easier. MATLAB integrates a Graphical User Interface (GUI), designed for fast design and analysis of processes with additional functionality with a programming language that is based on array and matrix mathematics. MATLAB can be utilized in fields of data science, machine learning, robotics, control system, power system analysis and design, embedded systems, computational biology, image processing, computer vision, wireless communications, enterprise and information technology (IT) systems, signal processing and so on.

Simulink is an integral part of MATLAB used for easy design and simulation. It is a block diagram based environment with automatic code generation and continuous test and verification. Simulink provides libraries with customisable blocks and solvers for simulating real time systems. Simscape Power System toolbox provides component libraries and analysis tools for modelling and simulating systems and circuits of electrical domain. It contains various library blocks that implements mathematical models of electrical equipment like resistors, inductors, electric machines, controllers, renewable energy systems and FACTS devices. Load flow, harmonic analysis, circuit design and verification and other analyses can be performed easily.

Simscape Power Systems toolbox also helps in development of control systems and analyse their performance. Many tasks as PI controller tuning are automated in Simulink. It can automatically generate parameter of a model using simulation results and numerous optimizers present in MATLAB. MATLAB can be interfaced with any physical system easily to collect data, apply digital control etc. For deploying control algorithms to embedded systems and other simulation environments, including hardware-in-the-loop (HIL) systems, Simscape supports C-code generation. The development of Simscape Power Systems is done with the help of Hydro-Québec of Montreal.

1.5 OUTLINE OF THE THESIS

The thesis contains following chapters:

Chapter 1 gives outline of broad area of Power Quality. Gives a brief on reasons and effects of Power Quality problems, existing standards and mitigation techniques. An introduction to software platform used for simulation and analysis is also given

Chapter 2 presents literature survey on Power Quality improvement using Static Synchronous Compensator (STATCOM). Various configurations and applications are reviewed. A brief survey on different STATCOM control algorithms is presented and objectives of present work are defined.

Chapter 3 presents application of sigmoid cost framework to LMS based algorithm for STATCOM control. STATCOM is implemented for mitigating Power Quality issues of harmonics and poor power factor. A comparison of performance of different sigmoid cost framework based algorithms is given.

Chapter 4 presents integration of solar Photo-Voltaic (PV) system with grid using STATCOM. A two stage control for PV-STATCOM system using incremental conductance algorithm and sigmoid cost framework based algorithm is implemented and analysed.

Chapter 5 presents conclusion of the thesis and scope of future work.

CHAPTER 2

LITERATURE SURVEY:
STATIC SYNCHRONOUS COMPENSATOR FOR POWER QUALITY IMPROVEMENT

The Static Synchronous Compensator (STATCOM) is a solid-state switching converter based device that absorbs or delivers active and reactive power in a regulated way. An energy source or energy storing element is connected at its input and its output can be changed to modify certain properties of an electrical system network. The energy storing element at its input can be either an inductor or a capacitor. When an inductor is connected at its input the converter works like a current source converter while for a capacitor at its input the converter act as a voltage source converter. Due to nature of most load, reactive power requirement and increased losses for high value of inductor, voltage source converter configuration are preferred [4].

Along with control of reactive power the STATCOM improves transient stability, power oscillations damping, dynamic voltage control and voltage flicker control [1][3]. Compared to conventional synchronous compensator STATCOM ideally has no inertia so its response is instantaneous and has very little effect on the system impedance. Its running and maintenance cost are also less. STATCOM are also used as cost effective Shunt Active Power Filter (SAPF) to reduce harmonics in the load current [4]. The STATCOM can be used for supplying active power from a DC energy source such as battery, Photo-Voltaic (PV) cells or fuel cells connected at its input.

2.1 OPERATION OF STATCOM

The STATCOM may be seen as a controlled reactive power source. The Voltage Source Converter (VSC) of STATCOM controls the exchange of reactive as well as active power between a utility bus and its energy storing element. Magnetic coupling as an inductor or transformer is used between he VSC and the utility bus through. In

single line diagram the STATCOM is represented as a controlled voltage source behind a impedance, depicted in Figure 2.1. By varying the magnitude of output voltage E_s of the converter, the reactive power transfer between the STATCOM and AC system is regulated. When the magnitude of voltage E_s is greater than bus voltage of utility E_t the STATCOM generates capacitive reactive power and flow of current is from the converter to utility. When magnitude of converter output voltage is less than utility voltage, then STATCOM absorbs inductive reactive power from the utility. There is no transfer of reactive power between STATCOM and utility, if both voltages are equal [3].

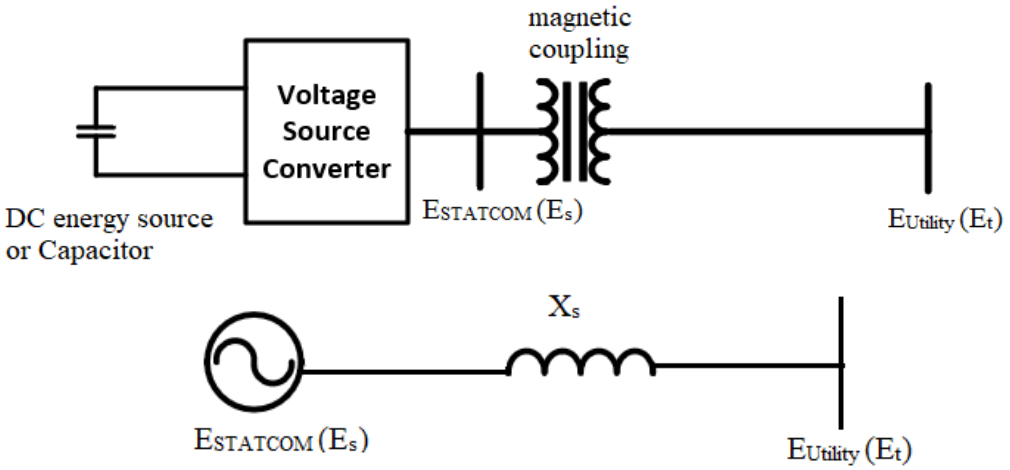

Fig. 2.1 STATCOM connected to utility bus

For exchange of active power between utility and STATCOM the phase difference between the STATCOM output and utility voltages is varied. If converter terminal voltage leads the utility voltage STATCOM supplies active power to the utility. If the utility voltage leads the converter terminal voltage, STATCOM absorbs active power. By transferring the instantaneous reactive power between the phases of AC system, the STATCOM provides reactive power. The converter interconnects the output terminals in a way that reactive current freely flows among them thus the converter creates a circular reactive power exchange system. The DC bus capacitor between the input terminals of the STATCOM provides a circulating path for reactive power exchange as well as act as a voltage source [5].

A single leg of VSC is shown in Figure 2.2 (a). The operation of single leg of VSC of STATCOM is shown by figure 2.2 (b). The first full cycle of AC waveform shows inverter operation of VSC during which device 1 and 4 conducts in first and second half cycles respectively. No diodes conduct during this interval. From the third half cycle the

device 4 turn-on and device 1 turn-off is delayed by 60°. In this mode current lags the voltage by 120° and VSC works in inverter mode. After one complete cycle of this mode of operation a delay of another 30° is applied and converter act as pure inductor. With further delays of 60°, 30°, 60°, 30° and 30° the operation of VSC as inductive rectifier, unity power factor rectifier, capacitive rectifier, pure capacitive operation and capacitive inverter is shown. The devices conducting are shown under the sinusoidal current waveform in figure 2.2 (b). Thus, by controlling firing angle we can control the STATCOM in inductive or capacitive range [1].

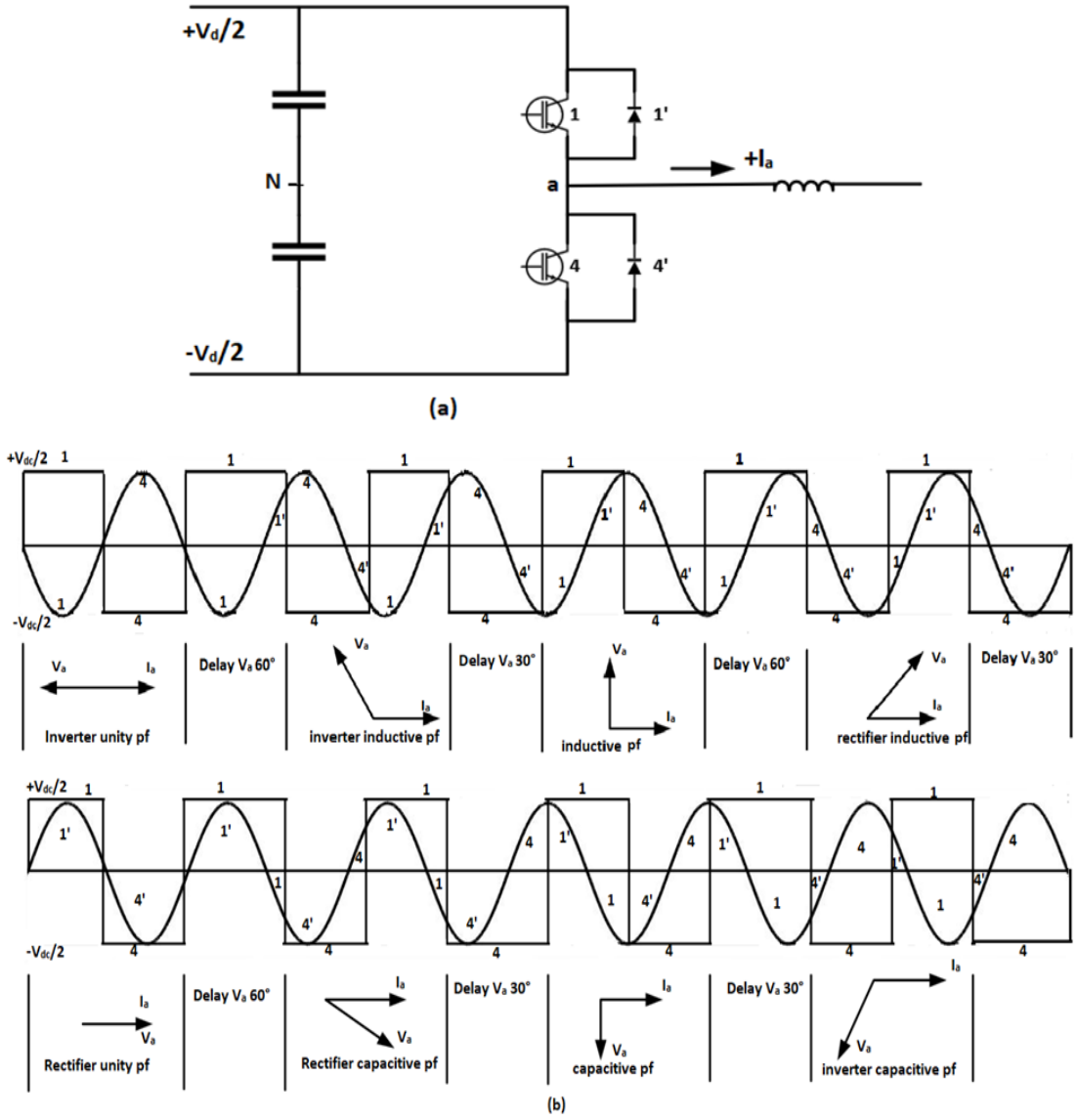

Fig. 2.2 Operation of VSC

2.2 STATCOM V-I CHARACTERISTIC

A generalised form of V-I characteristic of STATCOM is shown in figure 2.3. The STATCOM is capable of supplying both inductive as well as capacitive currents.

The STATCOM is capable of supplying capacitive currents even at very low system voltage. This property is useful for supporting system voltages during fault condition and recovering after fault.

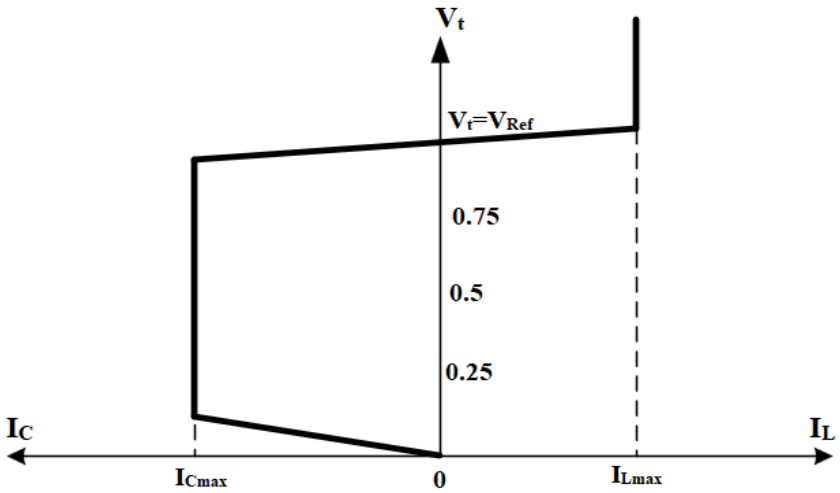

Fig. 2.3 STATCOM V-I characteristics

For the operation of STATCOM as a source off reactive power the capacitor at input remains charged at a reference voltage. In this case the VSC consumes real power from the AC terminals to maintain capacitor voltage constant. The STATCOM can supply and absorb both active and reactive powers this makes STATCOM ideal choice for improving system's dynamic performance and transient stability. Fig. 2.4 shows different conditions in which STATCOM operates [3].

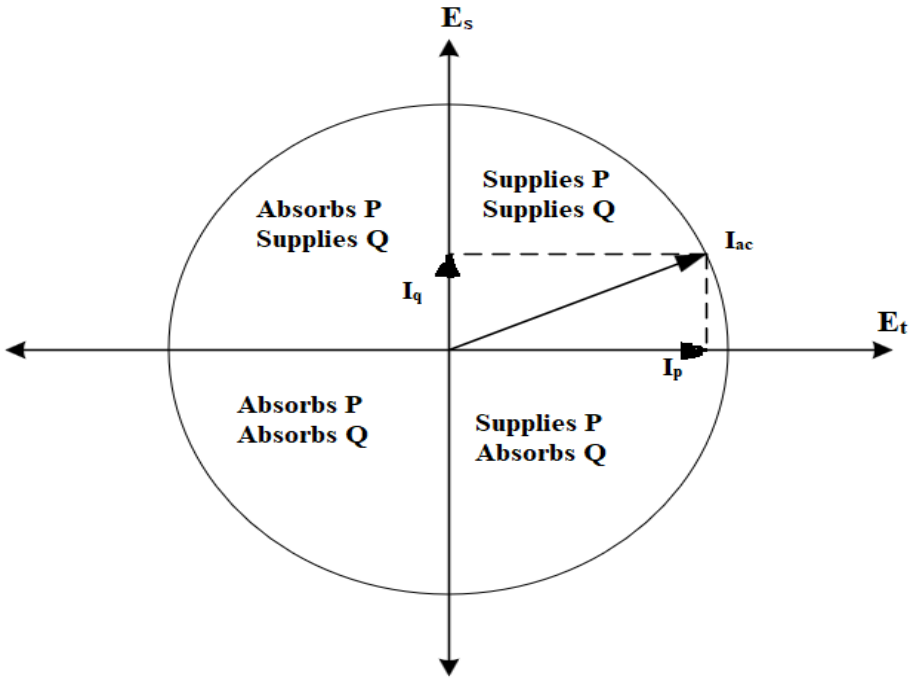

Fig. 2.4 Operation of STATCOM

2.3 CIRCUIT CONFIGURATIONS OF SHUNT CONNECTED STATCOM

Various configurations of DSTATCOM for three-phase and single-phase connections are present in literature [4] [11-16]. For single-phase system full-bridge and half-bridge circuit configurations of VSC based STATCOM are shown in figure 2.6 and 2.5 respectively.

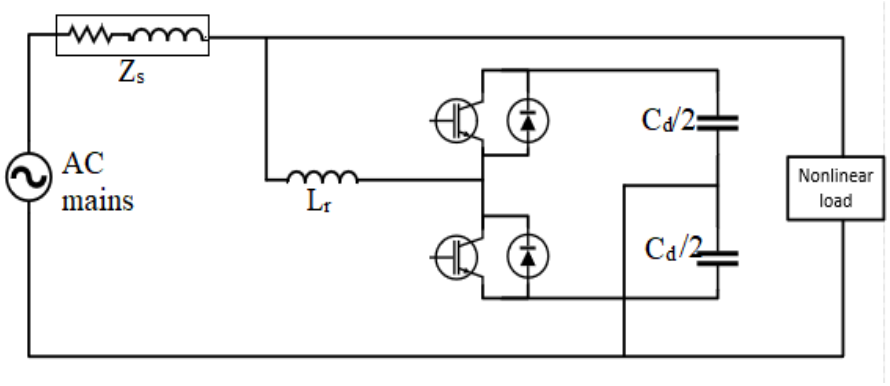

Fig. 2.5 Single-phase half-bridge STATCOM circuit configuration

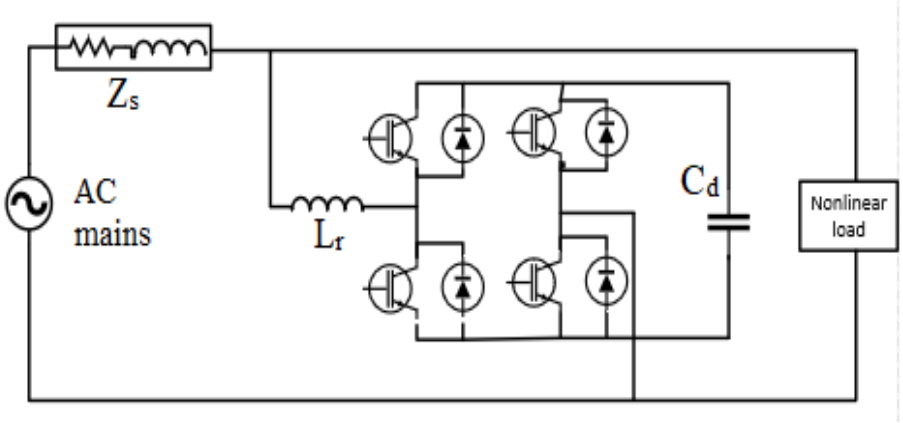

Fig. 2.6 Single-phase full-bridge STATCOM circuit configuration

Here Z_s is source impedance, L_r is interfacing inductor and C_d is DC bus capacitor. In half-bridge topology less number of switching devices are required than full-bridge. The rating of capacitor used in half-bridge circuit is also less than full bridge. For three-phase systems four-wire and three-wire connections, with or without isolating transformers are used [8]. Isolating transformer is required in case of high voltage applications. For three-phase three-wire system three-leg, three H-bridge and two-leg with split-capacitor configurations are implemented. For three-phase four-wire systems three-leg with split-capacitor [10], four leg, three-leg with Y-delta transformer and four

H-bridge type configurations are possible. Figure 2.7 and 2.8 shows a three-leg three-wire and three H-bridge four-wire STATCOM respectively.

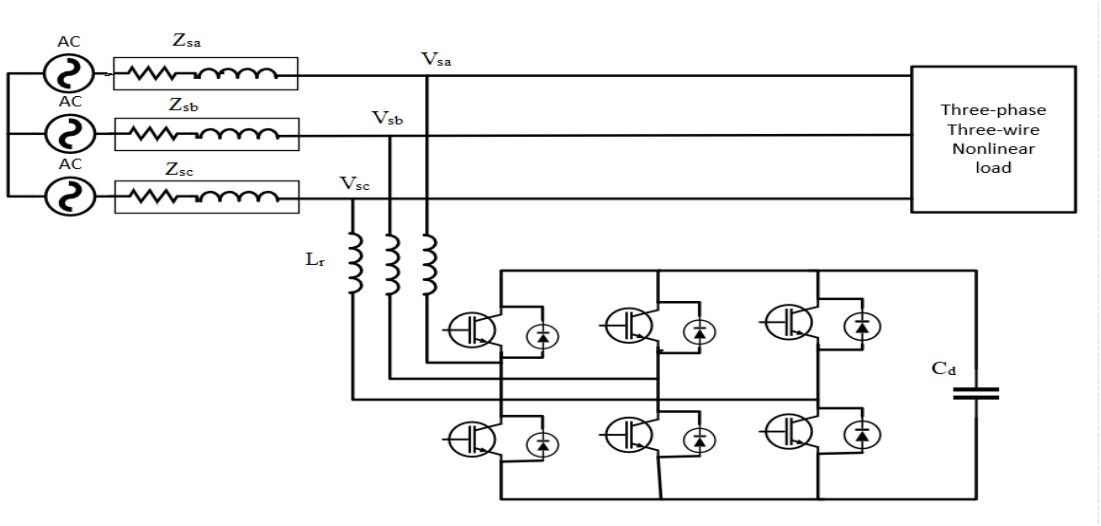

Fig. 2.7 Three-leg three-wire STATCOM configuration

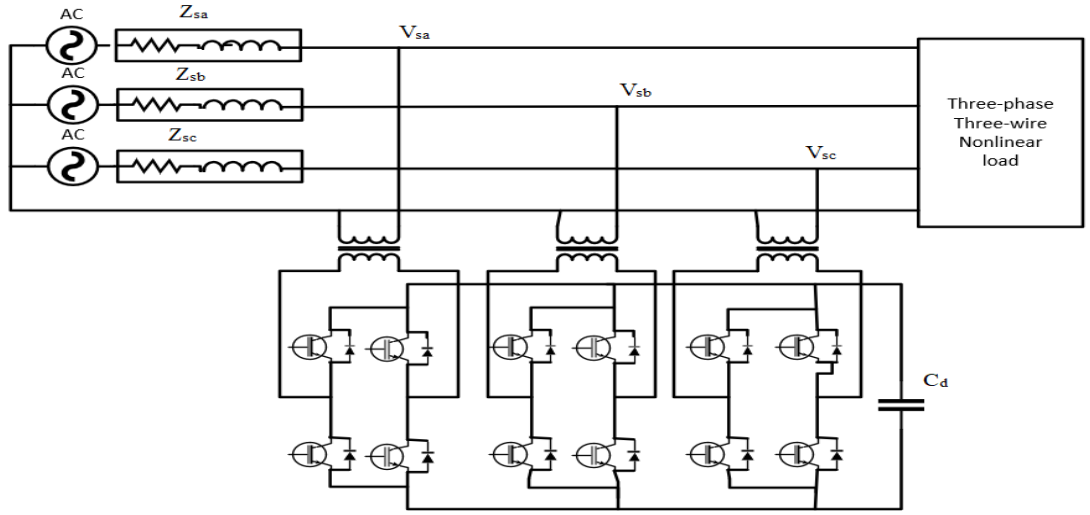

Fig. 2.8 Three H-bridge four-wire STATCOM configuration

Various other configurations for 3-phase 4-wire systems are presented in [11-14] and [16]. In [14] and [15] T-connected transformer based configuration are presented. In [16] Three-Phase Four-Wire STATCOM with Star/Hexagon Transformer configuration is implemented.

2.4 APPLICATIONS OF SHUNT CONNECTED STATCOM

STATCOM is used for many applications as mid-point voltage regulation, power oscillation damping, transient stability improvement and end-point voltage support in transmission lines. STATCOM can also act as an active power filter.

2.4.1 MID-POINT VOLTAGE REGULATION

In long transmission lines the voltage profile varies throughout the line due to line inductance and capacitance in loaded as well as unloaded condition [2]. STATCOM is used in shunt (ideally at mid-point) to maintain voltage profile by increasing the voltage at the mid-point. Figure 2.9 presents a single line representation and phasor diagram of mid-point compensated two bus system [1].

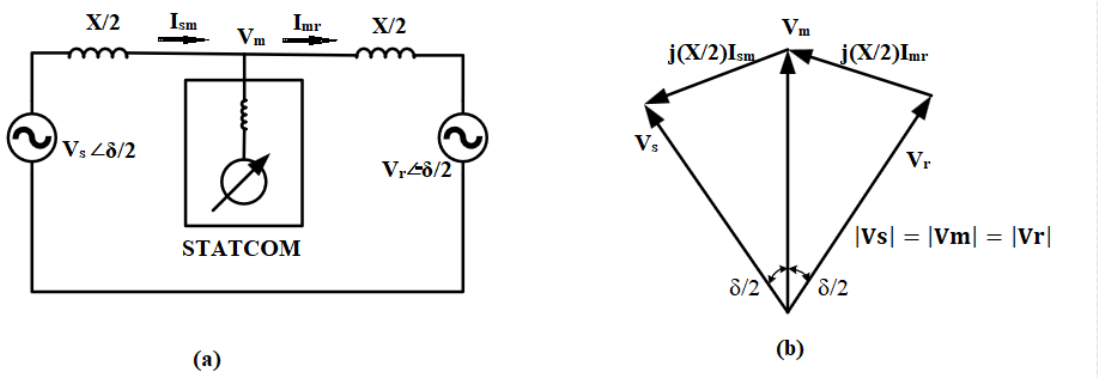

Fig. 2.9 STATCOM mid-point compensation and phasor diagram

2.4.2 END-POINT VOLTAGE STABILITY IMPROVEMENT

The voltage of load terminal of system highly depend in the power factor of the load. A generalised terminal voltage versus power plot with different load power factors for an uncompensated system is presented in Figure 2.10 (b). The plot shows that voltage stability limit with capacitive load, increase and decreases with inductive load. The STATCOM supplies reactive power demand of the load to maintain constant Point of Common Coupling (PCC) voltage. Fig. 2.10 (c) shows voltage versus power curve for compensated system. As shown in diagram, the voltage stability limit is improved with reactive shunt compensation [2].

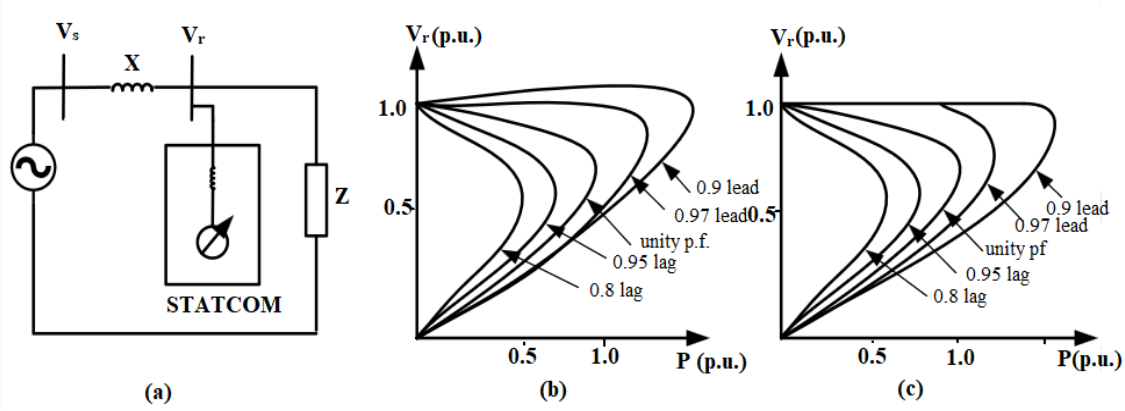

Fig. 2.10 STATCOM for load end voltage stability

2.4.3 TRANSIENT STABILITY IMPROVEMENT

The ability of supplying full capacitive current even with low system voltages makes STATCOM ideal for improving transient stability of the system. The maximum power transmission capacity of line can be increased using reactive shunt compensation [2]. Fig. 2.11 shows the curve between transmitted power and transmission angle for uncompensated and STATCOM compensated system with different ratings of STATCOM. The dotted line shows curve for uncompensated system [1]. Top curve shows curve for ideal shunt compensation. The curves in between show compensation by STATCOMs of different ratings. The curve show significant increase in transient stability margin area for curve with compensation for same value of transmission angle.

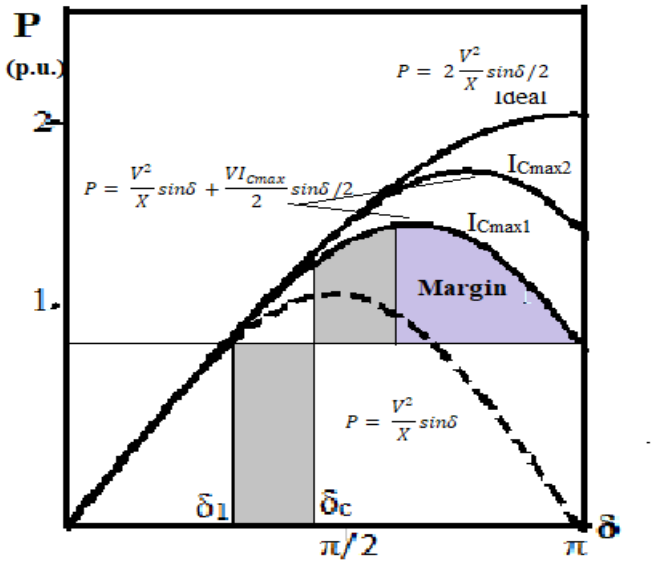

Fig. 2.11. Power versus transmission angle curve

2.4.4 DAMPING POWER OSCILLATIONS

For an underdamped power system due to a sudden disturbance the machine angle δ fluctuates between values around steady-state. This results in oscillations in power. With acceleration of generator, the angle δ increases. For compensating the surplus input mechanical power, the transmitted electric power must be increased. For a decelerating generator, angle δ decreases. To compensate the deficit input mechanical power the transmitted electric power must be decreased. As the STATCOM can dynamically vary mid-point voltage varying transmitted power it provides fast acting control for damping of power oscillations [1][2].

2.4.5 STATCOM FOR PV-GRID INTEGRATION

Rising global temperatures due to increased concentration of green house gases in the atmosphere and limited reserves of fossil fuel is forcing economies to move towards renewable sources of energy. The abundance and availability of solar radiation makes use of Photo-Voltaic (PV) cells for energy generation a viable option. The cost of generating power using PV panels have reduced significantly in last couple of decades. Nowadays small PV plants are installed by consumers, farmers, land owners for either their own needs or for commercial use. The integration of these plants with existing power system without causing power quality and stability issues is a huge challenge as the power generated by PV plants is not of AC type [29-31]. For small plants at distribution level STATCOM can be used for PV-Grid integration as well as power quality improvement in a cost-effective manner [32-33].

2.4.6 STATCOM AS SHUNT ACTIVE POWER FILTER

Shunt Active Power Filter (SAPF) is a dynamic and adjustable power-electronic based solution for power quality problems specially reduction of harmonic currents. Due to increased utilisation of solid-state based devices in consumer goods the problem of harmonic current has seen an exponential increase in the last couple of decades. The SAPF is connected in parallel with these non-linear loads to filter out harmonic currents. STATCOM with proper control methods is used as a cost effective SAPF as it can either supply or absorb active and reactive currents with the system [10-11] [15] [17].

2.5 CONTROL OF STATCOM AS SHUNT ACTIVE POWER FILTER

For generation of appropriate magnitude and waveform of currents, the switches of VSC of STATCOM are required to turn on and off at very high frequencies. Most popular solid state switches are Insulated-Gate Bipolar Transistor (IGBT) and Metal-Oxide Semiconductor Field Effect Transistor (MOSFET). They have a turn-on time of 100 ns for MOSFET and less than 1 μs for IGBT. Their turn off time is 200 ns and 2 μs for MOSFET and IGBT respectively. In both the gating pulse is voltage driven. The leakage current in MOSFET is 30 mA which is much larger than that of IGBT (<1

mA). MOSFETs can have switching frequencies of up-to 200 kHz while for IGBTs the range is 20 kHz to 50 kHz. IGBTs are preferred for high voltage (>1000 V) high allowable junction temperature (100 °C) and high output powers. MOSFET are used for low output powers and low voltage application (<250 V).

The turn off and turn on control of solid state switch at such high frequencies is only possible with the use of Digital Signal Processing (DSP) units. Many algorithms for control of SAPF have been developed over the years [17-28]. These algorithms are generally categorised as Time domain based and Frequency domain based. Some popular Time domain algorithms are:

1. Unit template technique or PI controller theory
2. d-q or Synchronous reference frame (SRF) theory [19]
3. α-β or Instantaneous reactive power theory (IRPT)
4. Widrow's LMS-based Adaline algorithm [21]
5. Power balance theory (BPT) [17]
6. Current synchronous detection (CSD) method [18]
7. Instantaneous symmetrical component theory (ISCT)
8. Enhanced phase-locked-loop (EPLL) based algorithm [20]
9. Conductance-based algorithm
10. Adaptive detecting control or adaptive interference cancelling theory

Frequency domain algorithm are computationally complex, resulting in slower performance than time domain algorithms. They are handy for monitoring power quality. Some Frequency domain algorithms are:

1. Fourier-series based theory
2. Wavelet transformation theory
3. Discrete Fourier-transform based theory
4. Stockwell transformation (S-transform) theory
5. Fast-Fourier-transform based theory
6. Hilbert–Huang transformation theory
7. Recursive-discrete Fourier-transform based theory
8. Empirical decomposition (EMD) transformation theory
9. Kalman filter-based control algorithm

In this work implementation of LMS based Adaline algorithm, for controlling a three-phase three-wire Distribution Static Synchronous Compensator (DSTATCOM).

2.5.1 LMS BASED ADALINE ALGORITHM

A number of Least Mean Square (LMS) based algorithm are available in many research works [21-28]. The basic idea behind the algorithm comes from the concept of adaptive Finite Impulse Response (FIR) filter. A general block diagram of adaptive FIR filter is presented in the figure 2.13. Here x_i are the input to the filter, y_k is the filtered output, d_k is the expected output, e_k is the error between desired and filtered output and w_k are weights estimated using an optimization algorithm to reduce the error between required and filtered response.

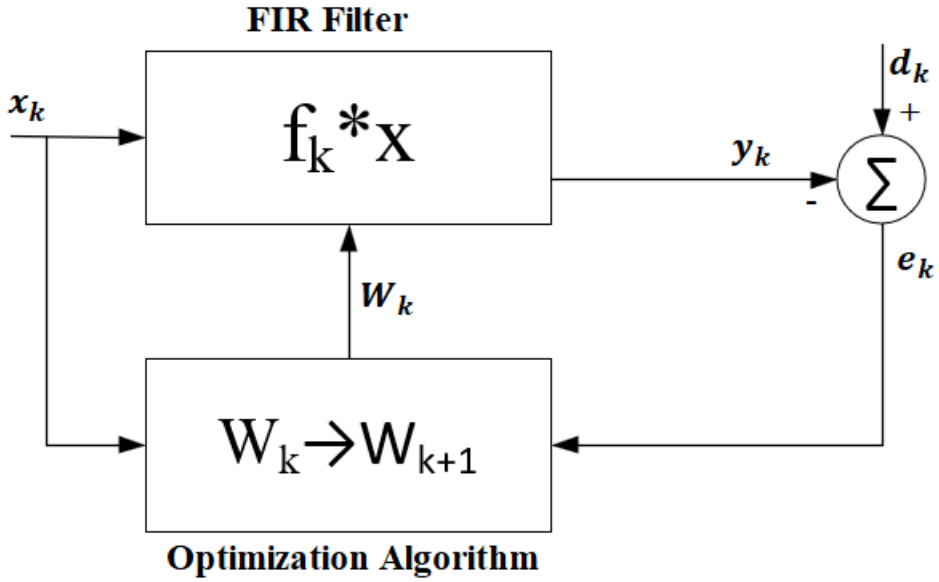

Fig. 2.13 General block diagram of adaptive filter

The above concept of adaptive filtering is utilised for determining the magnitude of fundamental-frequency component of load current. Gradient descent is the most popular optimization algorithm. The optimization algorithms use different cost functions to minimize the error. The Mean Squared Error (MSE) $E[e^2]$ is commonly used cost function. The weight update equation for LMS algorithm using above cost function is given as

$$W_{k+1} = W_k + \eta e_k x_k \tag{2.1}$$

Here,

$$e_k = d_k - x_k W_k \tag{2.2}$$

Here η is a parameter that controls the speed of weight update called convergence coefficient. High values of η cause stability problems and degrades algorithm performance.

Consider a three phase, three-wire DSTATCOM connected in parallel with three-phase load, supplied using a balanced three-phase source as shown in figure 2.14. For the purpose of controlling the DSTATCOM the source voltages ($v_{sa}, v_{sb,}\ v_{sc}$), source current (i_{sa}, i_{sb}, i_{sc}), load current (i_{La}, i_{Lb}, i_{Lc}) and DC capacitor voltage (V_{DC}) are measured and filtered to be utilised for feedback signals of the algorithm. The control algorithm can be divided into five steps as follows.

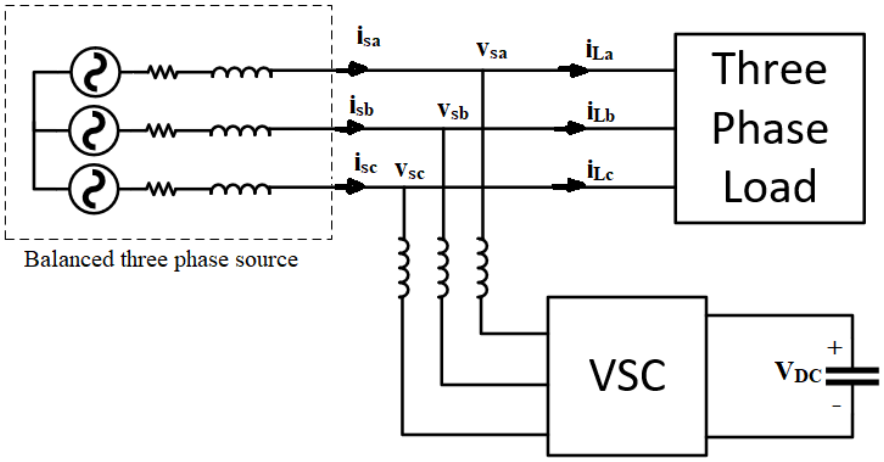

Fig. 2.14 Three phase three-wire DSTATCOM system

2.5.1.1 Calculation of direct and quadrature unit vector components of PCC voltages

For the application of improving Power Quality, the DSTATCOM is required to absorb or supply reactive power in the amount required by the system and achieve unity power factor at the PCC. For unity power factor the difference of phase angles of current and voltage phasors should be zero. The magnitude of AC voltage, the in-phase and quadrature unit vector calculation, using the measured PCC voltages, is done by equations 2.3, 2.4 and 2.5 respectively.

$$V = \sqrt{\frac{2}{3}(v_{sa}^2 + v_{sb}^2 + v_{sc}^2)} \tag{2.3}$$

$$u_{pa} = v_{sa}/V, \qquad u_{pb} = v_{sb}/V, \qquad u_{pc} = v_{sc}/V \tag{2.4}$$

$$u_{qa} = \frac{(u_{pc} - u_{pb})}{\sqrt{3}}, \quad u_{qb} = \frac{(3u_{pa} + u_{pb} - u_{pc})}{2\sqrt{3}}, \quad u_{qc} = \frac{(-3u_{pa} + u_{pb} - u_{pc})}{2\sqrt{3}} \tag{2.5}$$

2.5.1.2 Weight estimation of Direct and Quadrature Component of the Load Current

To eliminate the harmonics, the control algorithm extracts fundamental frequency in-phase (direct) and quadrature component of load current with respect to the source voltages. The weight values for each phase is estimated using weight update equation 2.1. The average of the three weight values of each phase is taken as final weight estimation (W_p and W_q) to balance three phase currents in case of unbalanced loading. The weight update equation are rewritten as

$$W_{pr(k+1)} = W_{pr(k)} + \eta\{i_{Lr(k)} - W_{pr(k)}u_{pr(k)}\}u_{pr(k)} \tag{2.6}$$

$$W_{qr(k+1)} = W_{qr(k)} + \eta\{i_{Lr(k)} - W_{qr(k)}u_{qr(k)}\}u_{qr(k)} \tag{2.7}$$

Here *r* can be phase 'a', 'b' or 'c'. *k* denotes the present iteration.

$$W_p = (W_{pa} + W_{pb} + W_{pc})/3 \tag{2.8}$$

$$W_q = (W_{qa} + W_{qb} + W_{qc})/3 \tag{2.9}$$

2.5.1.3 AC voltage and DC capacitor voltage regulation

The DC capacitor voltage (V_{DC}) is required to be maintained at a set reference value for operation of the DSTATCOM. A Proportional Integral (PI) control is utilised for this purpose. The sensed DC bus voltage is subtracted from the set voltage value and the error generated is passed through a PI controller. The equation for PI controller output is given as

$$i_{lDC} = K_{pDC}(V_{DC}^* - V_{DC}) + K_{iDC}\int(V_{DC}^* - V_{DC})dt \tag{2.10}$$

For regulating PCC voltage, the measured AC voltage magnitude by equation 2.3 is subtracted from a set reference value of voltage magnitude. The generated error is passed through a PI controller. The equation for PI controller output is given as

$$i_{lAC} = K_{pAC}(V_{AC}^* - V_{AC}) + K_{iAC}\int(V_{AC}^* - V_{AC})dt \tag{2.11}$$

2.5.1.4 Calculation of three phase reference Current

The PI controller output for DC capacitor voltage control is added to the weight value of direct component of load current (W_p) to obtain direct component of reference current.

$$i_p = W_p + i_{lDC} \tag{2.12}$$

The weight value of quadrature component of load current (W_q) is subtracted from the PI controller output for AC voltage regulation to obtain quadrature component of reference current.

$$i_q = -W_q + i_{lAC} \tag{2.12}$$

Using unit voltage (2.4-2.5) vectors and direct and quadrature component of reference current (2.12-2.13), final three-phase reference current are computed as

$$i_{sa}^* = i_p u_{pa} + i_q u_{qa}, \qquad i_{sb}^* = i_p u_{pb} + i_q u_{qb}, \qquad i_{sc}^* = i_p u_{pc} + i_q u_{qc} \tag{2.13}$$

2.5.1.5 Generation of Gate Signals for the IGBTs of DSTATCOM

The measured supply currents (i_{sa}, i_{sb}, i_{sc}) and the reference currents ($i_{sa}^*, i_{sb}^*, i_{sc}^*$) are processed in the hysteresis current controller [9] to generate switching signals for IGBTs of the DSTATCOM.

The LMS algorithm described above can be used for Unity Power Factor (UPF) mode as well as Zero Voltage Regulation (ZVR) mode of DSTATCOM operation with slight modification. The quadrature component of reference current obtained in equation 2.12 is set to zero, for UPF mode of operation. Other steps remain the same. The mathematical model described above is represented as a block diagram in figure 2.15.

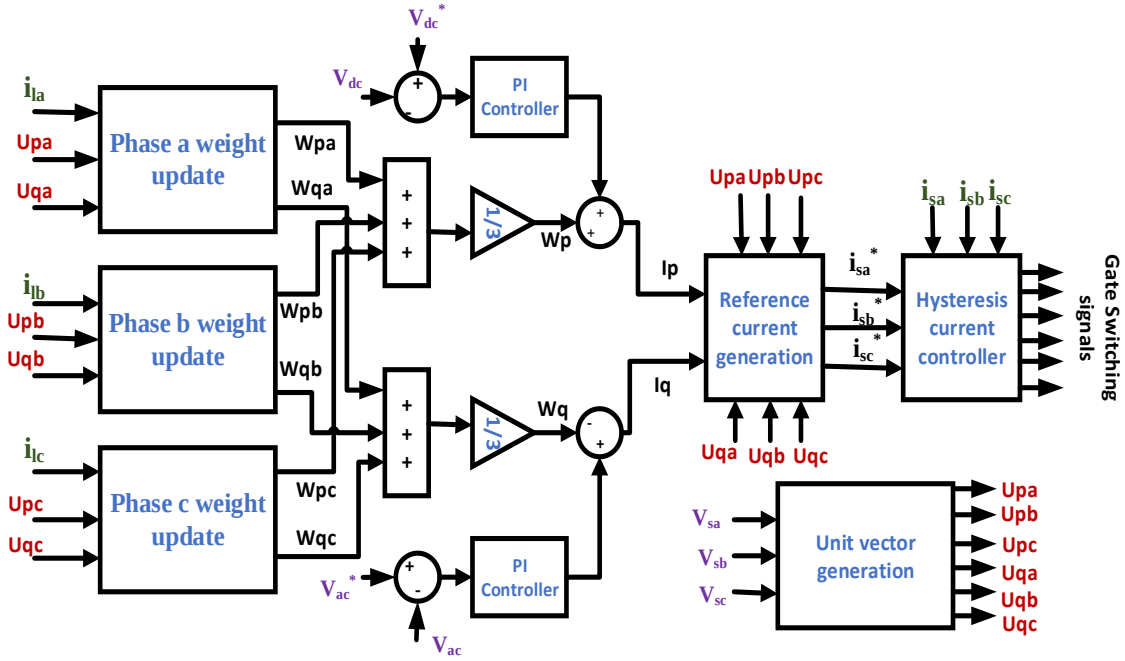

Fig. 2.15. Generalised block diagram representation of LMS algorithm

In literature many algorithms based on above concept have been proposed over the years with different type of cost functions or other modifications for different applications and scenarios. By using cost function as higher order of error, algorithms like 'Least Mean Fourth' (LMF) are developed. Using error in sign function 'Least Absolute Difference' (LAD) algorithm is developed. 'Least Mean Logarithmic Square' (LMLS) and 'Logarithmic Least Absolute Difference' (LLAD) algorithms are developed, based on logarithmic cost [27].

Many other algorithms are developed by using Recursive-Inverse theory and Variable Forgetting Factor (VFF) methods [26]. Variable step size LMS algorithms are presented in [24] and [25]. Each algorithm has its benefits and drawbacks in terms of speed, transient response, steady state performance, complexity etc.

2.6 PV-GRID INTEGRATION

With increasing penetration of solar PV plants their integration with conventional grid is a challenging area of research. Conventionally standalone PV plants used to supply local demands without any interaction with the grid [40]. Nowadays with increasing power demands, commercial generation using PV-plants and emphasis on renewable energy generation PV-grid integration is becoming common practice. As PV panels generate DC voltage and current suitable means of conversion are used for grid integration. Some conversion techniques for PV-grid integration are discussed in [30] using power electronics circuits. PV-DSTATCOM system for PV-grid integration is presented in [31-33] with various control methods as based on Enhanced Phase-Locked-Loop (EPLL), Quadrature-Oscillator based and adaptive filter based. As the output of PV panels vary with different factors a control method is required to extract maximum power available at any time. Different control methods are presented in [34-39]. Some methods of Maximum Power-Point Tracking (MPPT) are model-predictive control [34], Incremental-Conductance (IC) [35][37], Perturb and Observe (P&O) [35][36], Discrete time ripple correlation control [38] and Particle-Swarm Optimization (PSO) [38].

2.7 OBJECTIVES OF CURRENT WORK

1. To address Distribution System's Power Quality issues
2. Implement a SAPF in a Three phase three-wire system

3. Design a boost converter for PV- DSTATCOM system for PV-grid integration
4. Implement Incremental conductance MPPT control
5. To implement Sigmoidal Least Mean Square (SLMS), Sigmoidal Least Mean Fourth (SLMF), Sigmoidal Least Absolute Difference (SLAD), Sigmoidal Logarithmic Least Absolute Difference (SLLAD) and Sigmoidal Least Mean Logarithmic Square (SLMLS) algorithms for DSTATCOM control
6. Modification of control algorithm for integration of PV with distribution system

2.8 CHAPTER SUMMARY

In this chapter STATCOM, it's operation, application and control for power quality improvement are reviewed. Various control algorithms for STATCOM control are reviewed and basics of LMS based algorithm are presented. Various methods for PV-grid integration are also reviewed. Objectives of current work are defined.

CHAPTER 3

DSTATCOM CONTROL FOR POWER QUALITY IMPROVEMENT WITH SIGMOID BASED ALGORITHMS

3.1 SIGMOID COST FRAMEWORK BASED ALGORITHMS

For improvement in the robustness of algorithms based on LMS which uses higher-order statistics and to improve the steady-state performance by using lower-order statistics, a modified robust cost function using sigmoid framework is proposed in [28]. The new framework is resulted by 'inserting the conventional cost function into the sigmoid framework, which is used as a cost function'. These algorithm aims to improve the performance in terms of steady-state performance or convergence rate and improve robustness against impulsive interferences utilizing the saturation property of the nonlinear sigmoid function. Using the given sigmoid cost function, several conventional cost functions algorithms are modified into robust adaptive algorithms, such as the 'sigmoid least absolute difference' (SLAD), 'sigmoid least logarithmic absolute difference' (SLLAD), 'sigmoid least mean square' (SLMS), 'sigmoid least mean logarithmic square' (SLMLS) and 'sigmoid least mean fourth' (SLMF) algorithms.

3.1.1 SIGMOID LEAST MEAN SQUARE (SLMS) ALGORITHM

For LMS algorithm the cost function is $J(e_k) = E[e_k^2]$. Imbedding the cost function into the sigmoid cost framework, we get the update equation of the weight vector of Sigmoid least mean square (SLMS) algorithm [28]. The weight vector update equation for SAPF control given by equation (2.6) and (2.7) for LMS algorithm can be rewritten for SLMS algorithm as

$$W_{p(k+1)} = W_{p(k)} + \eta S_k(1 - S_k)e_k u_{p(k)} \tag{3.1}$$

$$W_{q(k+1)} = W_{q(k)} + \eta S_k(1 - S_k)e_k u_{q(k)} \tag{3.2}$$

Where $S_k = sgm[\alpha e_k^2] = \frac{1}{1+e^{-\alpha e_k^2}}$ (3.3)

and, $e_k = i_{L(k)} - W_{(k)}u_{(k)}$ (3.4)

α is a positive parameter that controls the steepness of the sigmoid function. Whenever the impulsive interferences occur, the system output error is very large so that S_k approaches to one and eventually leading to $S_k(1 - S_k)$ tends to zero. As a result, the very small $S_k(1 - S_k)$ and the very large e_k counteract each other to give more robust performance.

3.1.2 SIGMOID LEAST ABSOLUTE DIFFERENCE (SLAD) ALGORITHM

The least absolute difference algorithm is derived using the cost function $J(e_k) = \{E[|e_k|]$. Imbedding it into the sigmoidal cost we get the update equations of the weight vectors for SLAD algorithm as

$$W_{p(k+1)} = W_{p(k)} + \eta S_k(1 - S_k)sgn(e_k)u_{p(k)} \quad (3.5)$$

$$W_{q(k+1)} = W_{q(k)} + \eta S_k(1 - S_k)sgn(e_k)u_{q(k)} \quad (3.6)$$

Here, $S_k = \frac{1}{1+e^{-\alpha|e_k|}}$ (3.7)

and $e_k = i_{L(k)} - W_{(k)}u_{(k)}$ (3.8)

3.1.3 SIGMOID LEAST MEAN FOURTH (SLMF) ALGORITHM

The least mean fourth algorithm is derived using the cost function $J(e_k) = E[e_k^4]$. Imbedding it into the sigmoidal cost we get the update equations of the weight vectors for SLMF algorithm as

$$W_{p(k+1)} = W_{p(k)} + \eta S_k(1 - S_k)e_k^3 u_{p(k)} \quad (3.9)$$

$$W_{q(k+1)} = W_{q(k)} + \eta S_k(1 - S_k)e_k^3 u_{q(k)} \quad (3.10)$$

Here, $S_k = \frac{1}{1+e^{-\alpha e_k^4}}$ (3.11)

and $e_k = i_{L(k)} - W_{(k)}u_{(k)}$ (3.12)

3.1.4 SIGMOID LEAST LOGARITHMIC ABSOLUTE DIFFERENCE (SLLAD) ALGORITHM

The LLAD algorithm is based on the cost function $J(e_k) = \{E|e_k^2| - (1/\beta)(\ln(1+\beta E|e_k^2|))\}$. where value of β is always positive. Imbedding it into the sigmoidal cost we get the equations of the weight estimation for SLLAD algorithm as

$$W_{p(k+1)} = W_{p(k)} + \eta S_k(1-S_k)\frac{\beta e_k u_{p(k)}}{1+\beta|e_k|} \tag{3.13}$$

$$W_{q(k+1)} = W_{q(k)} + \eta S_k(1-S_k)\frac{\beta e_k u_{q(k)}}{1+\beta|e_k|} \tag{3.14}$$

Here, $$S_k = \frac{1}{1+e^{-\alpha[|e_k|-(1/\beta)\ln(1+\beta|e_k|)}} \tag{3.15}$$

and $$e_k = i_{L(k)} - W_{(k)}u_{(k)} \tag{3.16}$$

3.1.5 SIGMOID LEAST MEAN LOGARITHMIC SQUARE (SLMLS) ALGORITHM

The LMLS algorithm is based on the cost function $J(e_k) = \{E[e_k^2] - (1/\beta)(\ln(1+\beta E[e_k^2]))\}$. Here value of β is always positive. Imbedding it into the sigmoidal cost we get the equations of weight estimation for SLMLS algorithm as

$$W_{p(k+1)} = W_{p(k)} + \eta S_k(1-S_k)\frac{\beta e_k^3 u_{p(k)}}{1+\beta e_k^2} \tag{3.17}$$

$$W_{q(k+1)} = W_{q(k)} + \eta S_k(1-S_k)\frac{\beta e_k^3 u_{q(k)}}{1+\beta e_k^2} \tag{3.18}$$

Here, $$S_k = \frac{1}{1+e^{-\alpha[e_k^2-(1/\beta)\ln\left(1+\beta e_k^2\right)}} \tag{3.19}$$

and $$e_k = i_{L(k)} - W_{(k)}u_{(k)} \tag{3.20}$$

3.2 DESIGN AND IMPLEMENTATION OF THREE PHASE DISTRIBUTION SYSTEM WITH DSTATCOM

For this study a three phase three-wire distribution system with DSTATCOM for improving power quality, is implemented and analysed using MATLAB. The proposed circuit configuration of the system is given in figure 3.1.

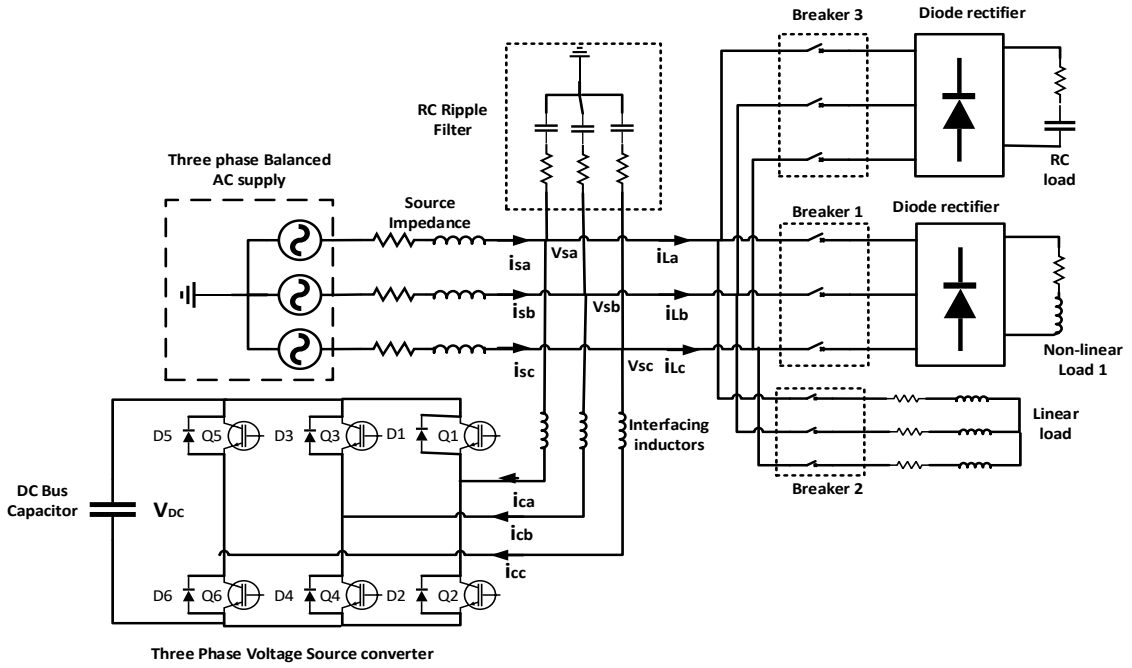

Fig. 3.1. Circuit diagram of proposed system

3.2.1 DESIGN AND MODELLING OF SUPPLY AND LOADS

The common supply system voltage at distribution level is 415 V line-to-line. The system frequency is chosen as 50 Hz. The supply system may be designed by a three phase balanced source with source inductance. In MATLAB the supply system is implemented using Simulink library block 'Three-Phase Source' in series with a 'Series RLC Branch' available in Simscape Power System toolbox. The configuration of three phase source is selected as star-grounded. The value of resistance, inductance and capacitance of series RLC branch is selected as 0.1 Ω, 1 mH and 0 F.

To study effects on power quality in various conditions different types of load are parallelly connected with each other using circuit breakers. A non-linear load is implemented using a 'Universal Bridge' block and a 'Series RLC Branch'. The 'Power Electronic device' option is set to diodes. The series RLC branch is placed at DC terminals of universal bridge. The value of capacitance is set to zero. A linear load is implemented using 'Series RLC Branch' connected in star configuration with value of capacitance set to zero as most of the loads in general are of resistive-inductive type. A capacitive load connected at the DC side of 'Universal Bridge' is used to simulate impulsive load behaviour. The MATLAB diagram of system is presented in figure 3.2.

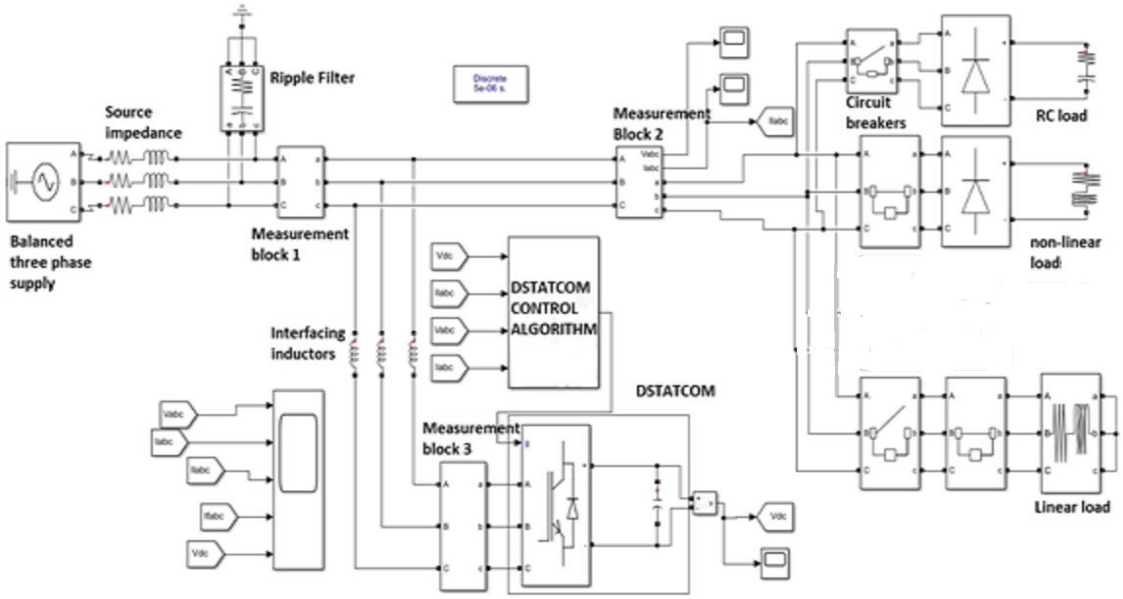

Fig. 3.2. MATLAB implementation of system

3.2.2 DESIGN AND MODELLING OF DSTATCOM

For the three phase system three-leg three-wire DSTATCOM with six switching devices can be used. IGBT with antiparallel diodes are used as switching devices for the VSC. In MATLAB the converter is implemented using 'Universal Bridge' block with 'Power Electronic devices' set to 'IGBT / Diodes' and 'Number of bridge arms' set to three. For the operation of VSC the voltage across the capacitor (DC bus) should remain fixed at a set reference value. The reference voltage's minimum value across the DC bus capacitor is derived using

$$V_{DC} = \frac{2\sqrt{2}V_{LL}}{\sqrt{3}} \tag{3.21}$$

The selected line-to-line voltage (V_{LL}) value is 415 V. V_{DC} evaluates to 677.69 V. For convenience value of DC capacitor reference voltage is selected as 700 V. The DC bus capacitor value can be obtained in many ways. Here the capacitance is calculated based on the ripples across the capacitor voltage, as

$$C_{DC} = \frac{I_0}{2\omega V_{DC,pp}} \tag{3.22}$$

Here ω is the frequency in radians, I_0 is the current through capacitor and $V_{DC,pp}$ is the voltage ripple across capacitor. Assuming the ripple as 1 %, $V_{DC,pp}$ = (0.01 x 700) = 7 V. For a 40000 VAR DSTATCOM current through DC bus capacitor I_0 =

(40000 / 700) = 57.14 A. With a safety factor of 10 % maximum current, I_0 = (1.1 x 57.14) = 62.85 A. With above values C_{DC} is obtained as 14290.75 μF. Thus, the value capacitance C_{DC} is chosen to be 15000 μF.

Interfacing inductors are used to reduce ripples in compensator currents. The AC inductance value for phase is selected based on the switching frequency, current ripple $I_{cr,pp}$ and DC bus voltage. The AC filter inductance is calculated as

$$L_r = \frac{\sqrt{3}mV_{DC}}{12af_sI_{cr,pp}} \tag{3.33}$$

Assuming a 10 % ripple in current, f_s = 25 kHz, m = 1, V_{DC} = 700 V, and a = 1, L_r is obtained as around near 0.808 mH. Here the value of interfacing inductors is selected as 1 mH.

To filter the high-frequency noise, generated from the switching of IGBT of DSTATCOM from the PCC voltage, a first-order low-pass filter tuned at half the switching frequency is connected. The capacitor of ripple filter is designed as C_f = 10 μF with series resistance R_f of 5 Ω. The RC filter is implemented in MATLAB using 'Series RLC Branch' and connected at PCC as shown in figure 3.2.

3.3 IMPLEMENTATION OF DSTATCOM CONTROL ALGORITHMS

The common diagram of blocks in LMS based algorithms is given in figure 2.15. The block diagram shows four major blocks: Unit vector generation block, hysteresis current controller block, block for generating reference current and weight estimation block.

3.3.1 UNIT VECTOR GENERATION BLOCK

The unit quadrature and in-phase voltage vector are derived from measured PCC voltage using measurement block 1 shown in figure 3.2. The MATLAB implementation of the block is shown in figure 3.3.

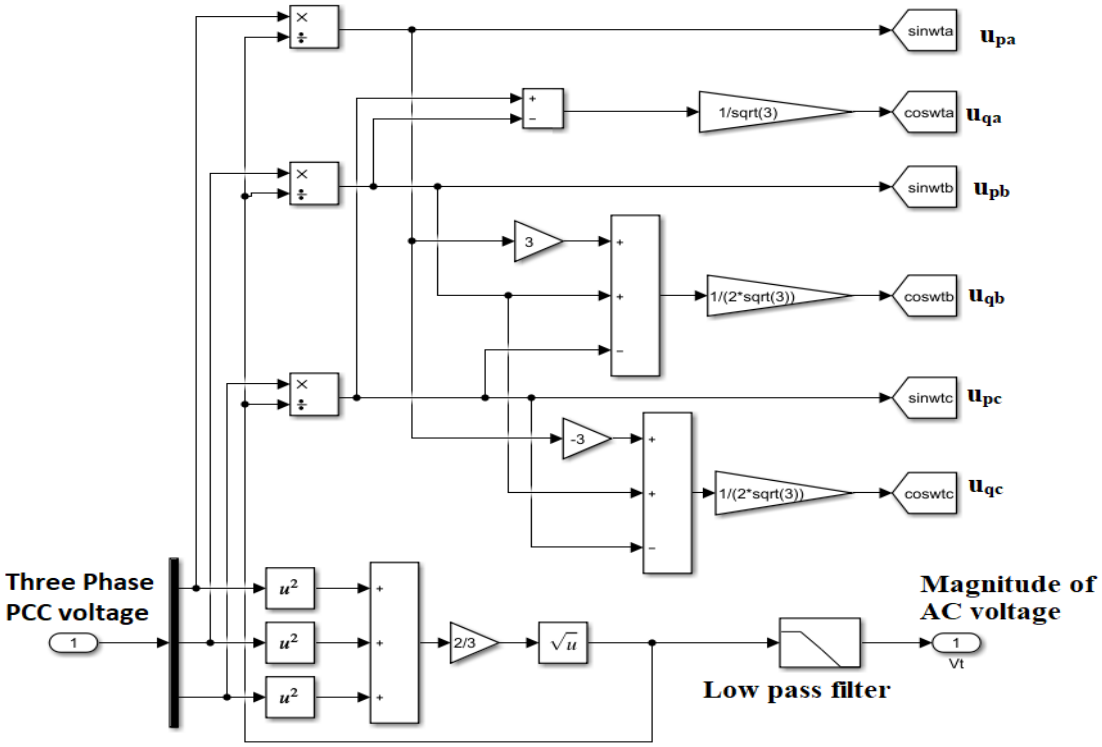

Fig. 3.3. MATLAB implementation of unit vector generation block

3.3.2 BLOCK FOR GENERATING REFERENCE CURRENT

The MATLAB implementation of block for generating reference current is given in Figure 3.4. with direct and quadrature component of reference current and unit vectors as input and three phase reference current as output.

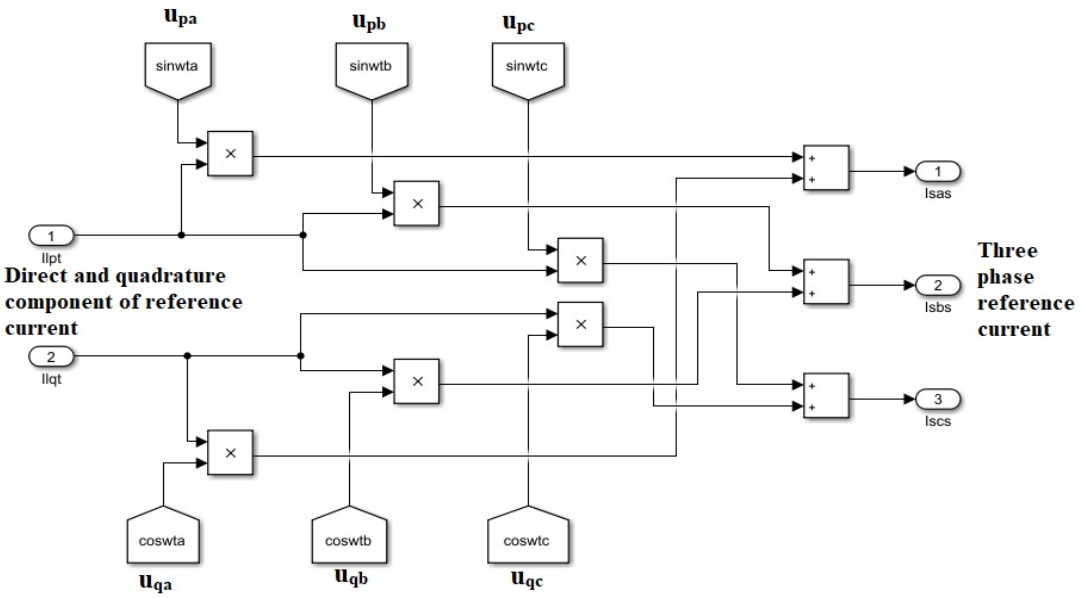

Fig. 3.4. MATLAB implementation of block for generating reference current

3.3.3 HYSTERESIS CURRENT CONTROLLER

Figure 3.5 shows hysteresis current controller block in MATLAB with three phase reference current and measured source current as inputs and switching signals as output.

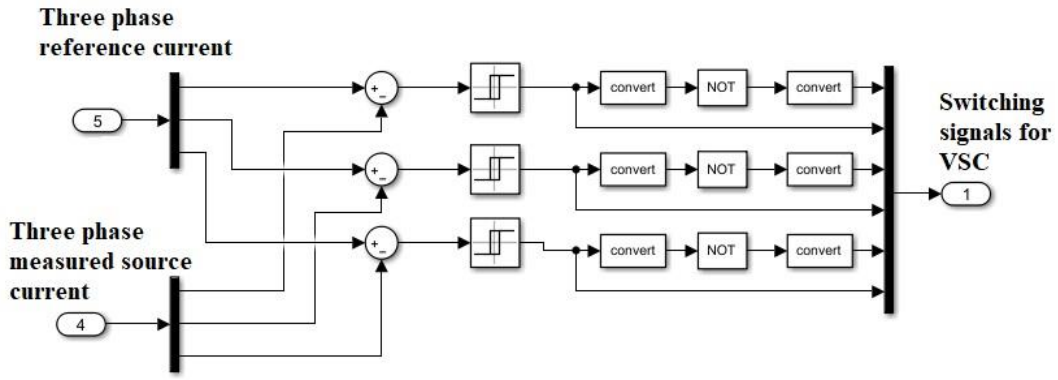

Fig. 3.5. MATLAB implementation of hysteresis current controller

3.3.4 WEIGHT ESTIMATION BLOCKS FOR DIFFERENT ALGORITHMS

The algorithms discussed in section 2.5.1 and 3.1 differs from each other in method of weight estimation.

3.3.4.1 LMS-Adaline Algorithm: The MATLAB implementation of weight estimation block for a single phase is given in figure 3.6, with inputs as measured phase load current and unit voltage vectors for that phase and load current's fundamental direct and quadrature component as outputs.

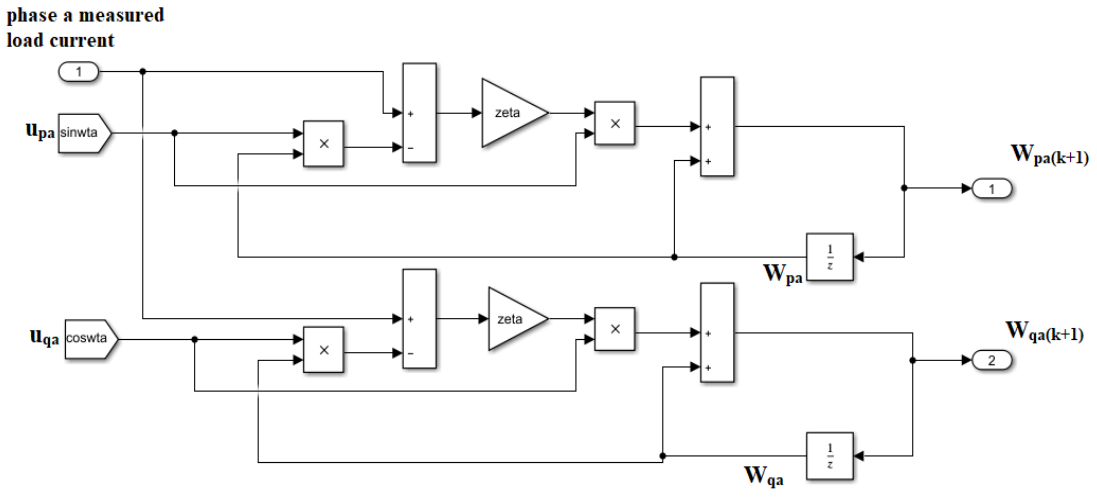

Fig. 3.6. MATLAB implementation of weight estimation for LMS-Adaline algorithm

3.3.4.2 Sigmoid Least Mean Square Algorithm: Figure 3.7 gives a MATLAB implementation of weight estimation block for SLMS algorithm.

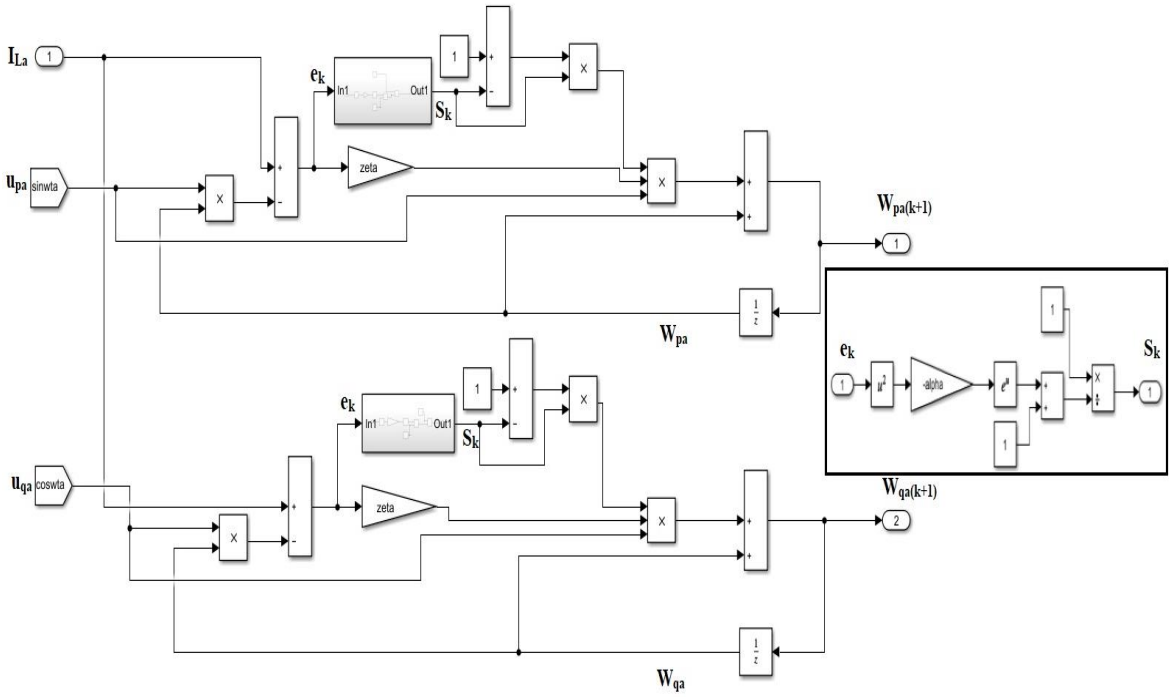

Fig. 3.7. MATLAB implementation of weight estimation for SLMS algorithm

3.3.4.3 Sigmoid Least Absolute Difference Algorithm: Figure 3.8 shows the MATLAB implementation of weight estimation block for SLAD algorithm.

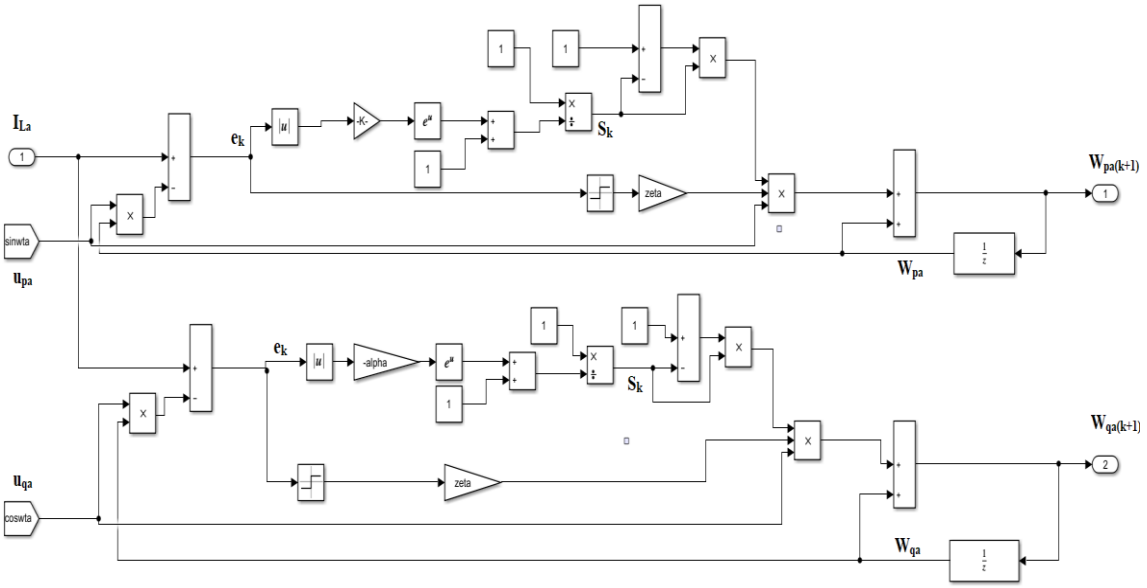

Fig. 3.8. MATLAB implementation of weight estimation for SLAD algorithm

3.3.4.4 Sigmoid Least Mean Fourth Algorithm: The MATLAB implementation of weight estimation block for SLAD algorithm is shown in Figure 3.9.

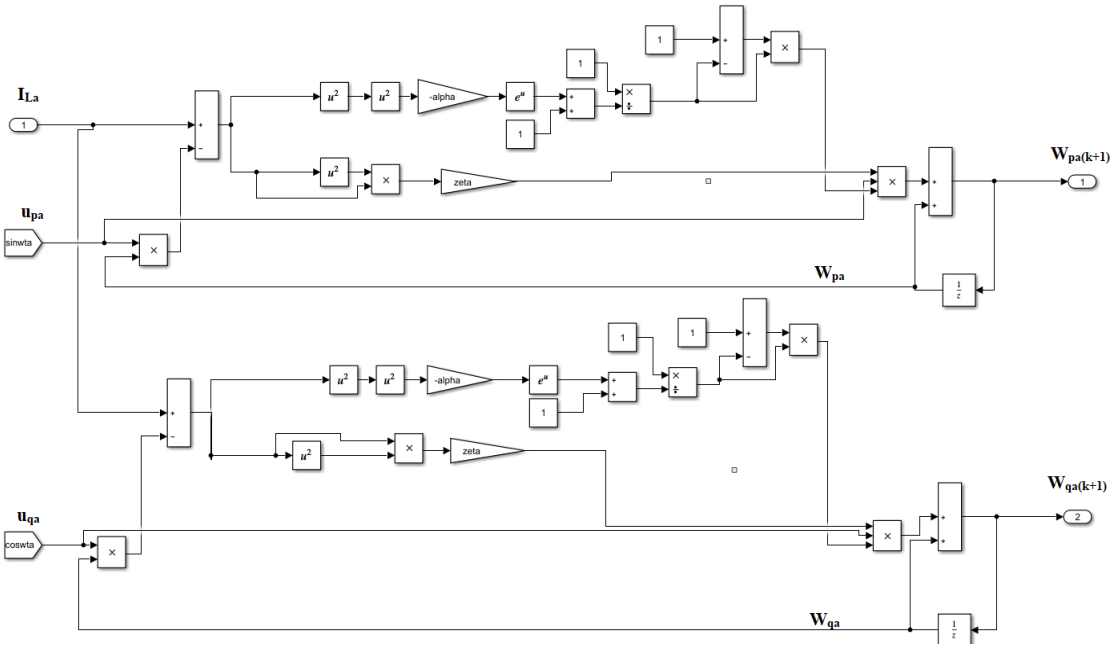

Fig. 3.9. MATLAB implementation of weight estimation for SLMF algorithm

3.3.4.5 Sigmoid Logarithmic Least Absolute Difference Algorithm: Figure 3.10 shows the MATLAB implementation of weight estimation block for SLLAD algorithm.

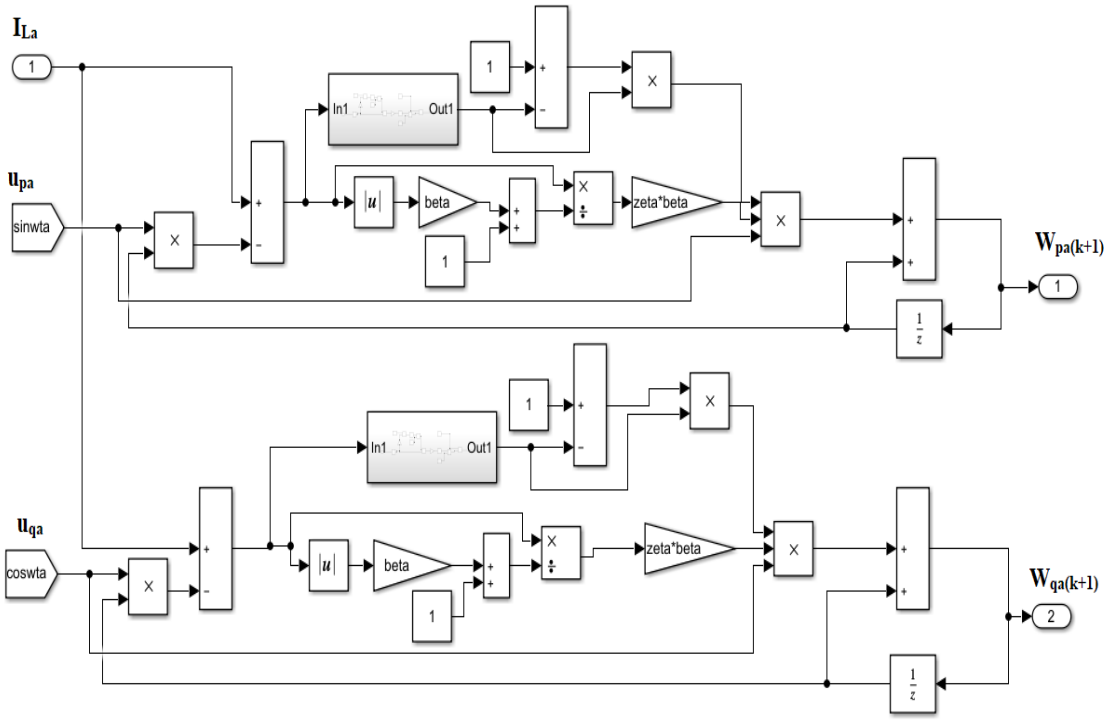

Fig. 3.10. MATLAB implementation of weight estimation for SLLAD algorithm

3.3.4.5 Sigmoid Least Mean Logarithmic Square Algorithm: Figure 3.11 shows the MATLAB implementation of weight estimation block for SLMLS algorithm.

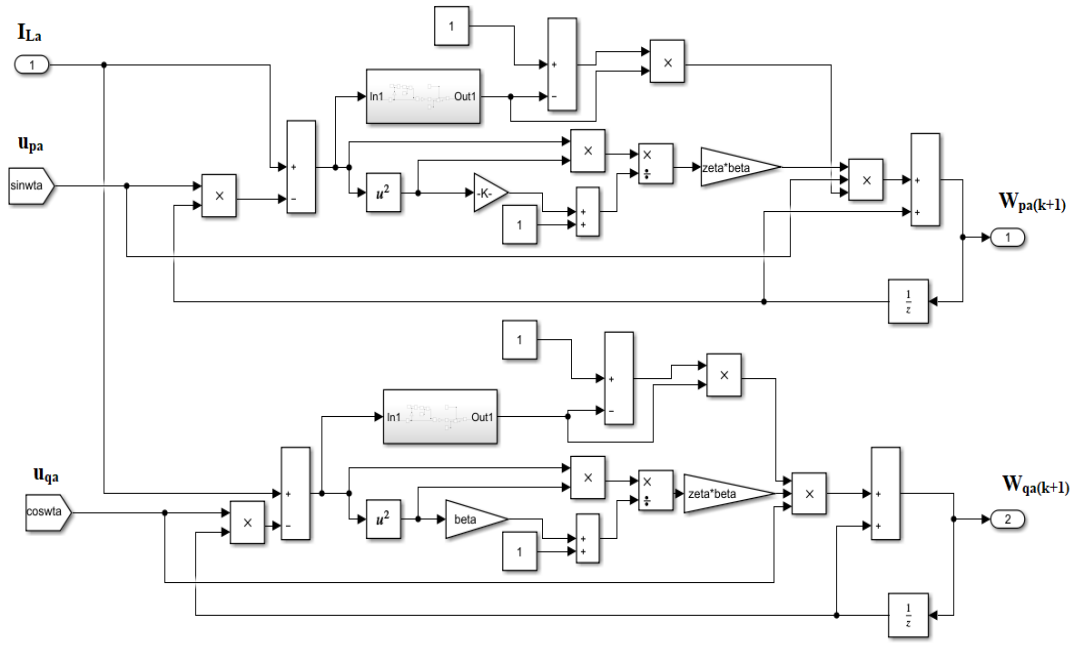

Fig. 3.11. MATLAB implementation of weight estimation for SLMLS algorithm

Figure 3.12 shows the overall MATLAB implementation of control algorithm with inputs load current, DC bus voltage, source current and voltage.

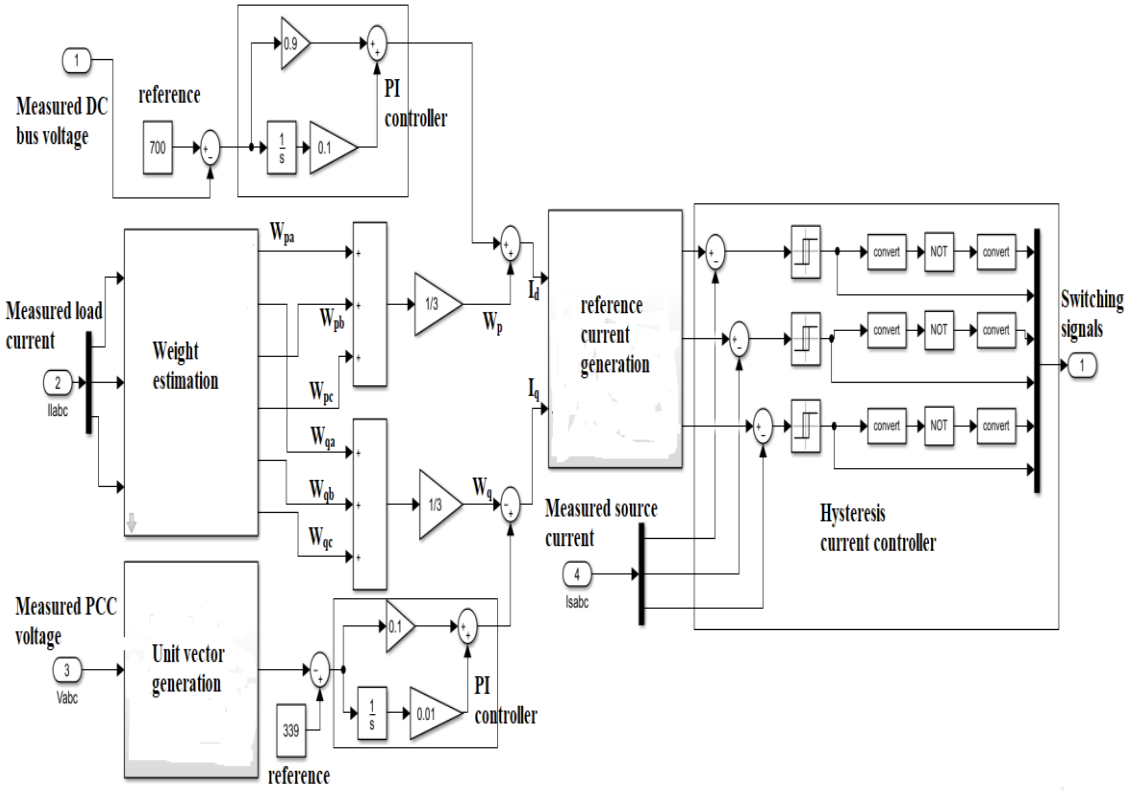

Fig. 3.12. MATLAB implementation of control algorithm

3.4 SIMULATION RESULTS AND DISCUSSION

Adaline-LMS, SLMS, SLAD, SLMF, SLLAD and SLMLS algorithms are simulated for improving Power Quality of system shown in figure 3.1. In powergui block simulation type is set to discrete and sample time is set to 5e-6. The value of inductor and resistor connected at the output of diode rectifier are 20 mH and 20 Ω respectively. The value of resistor and inductor of per-phase of three phase linear load is 10 Ω and 10 mH respectively. The value of resistor and capacitor connected at the end of diode rectifier are 1 Ω and 5000 μF respectively. Breaker 1 closed at 0 seconds and opened at 0.45 seconds. Breaker 2 is closed at 0.15 seconds and load is mixture of linear and non-linear load between 0.15 seconds and 0.3 seconds. Before 0.15 seconds load is purely non-linear. At 0.3 seconds phase 'a' of breaker 2 is opened and load is unbalanced between 0.3 seconds and 0.45 seconds. At 0.45 seconds Phase 'a' of breaker 2 is closed and load is purely linear.

3.4.1 RESULTS FOR ADALINE-LMS ALGORITHM

Figure 3.13 shows the source voltage (phase to ground) V_{Sabc}, current I_{Sabc}, load current I_{Labc}, DSTATCOM current I_{Cabc} and DC bus voltage V_{DC} for Adaline-LMS algorithm. The value of η in this case is 0.001.

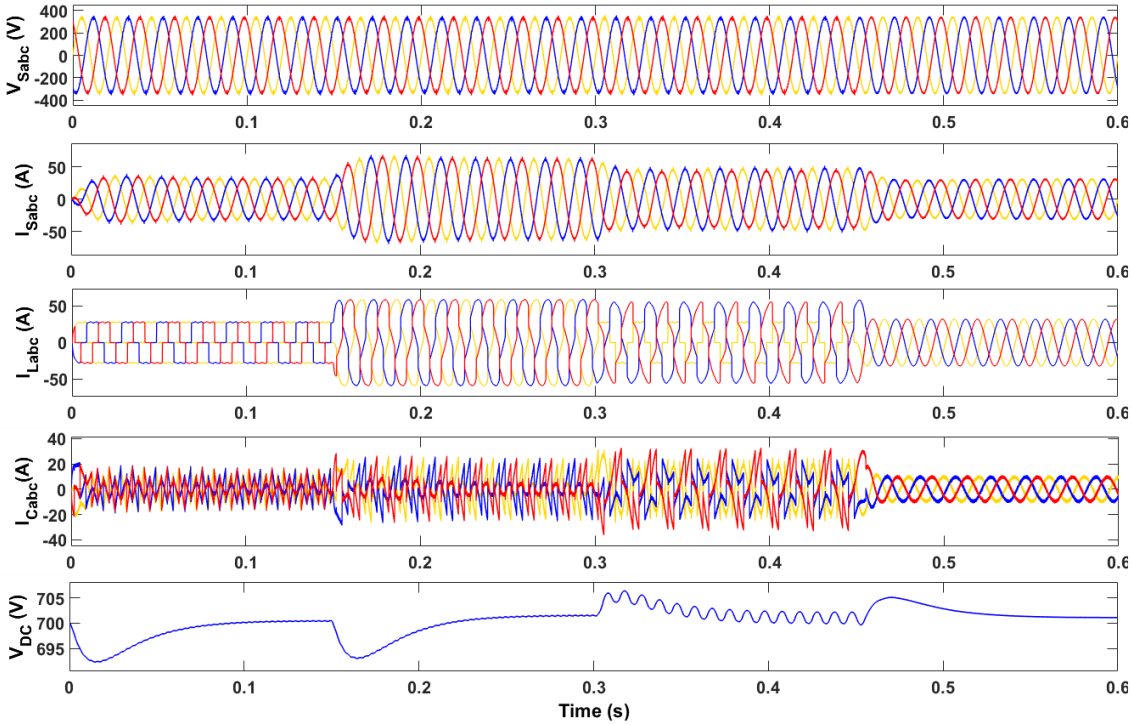

Fig. 3.13. Results for Adaline-LMS

3.4.2 RESULTS FOR SLMS ALGORITHM

The results for SLMS algorithm are shown in figure 3.14. The values of η and α are 0.003 and 0.001 respectively.

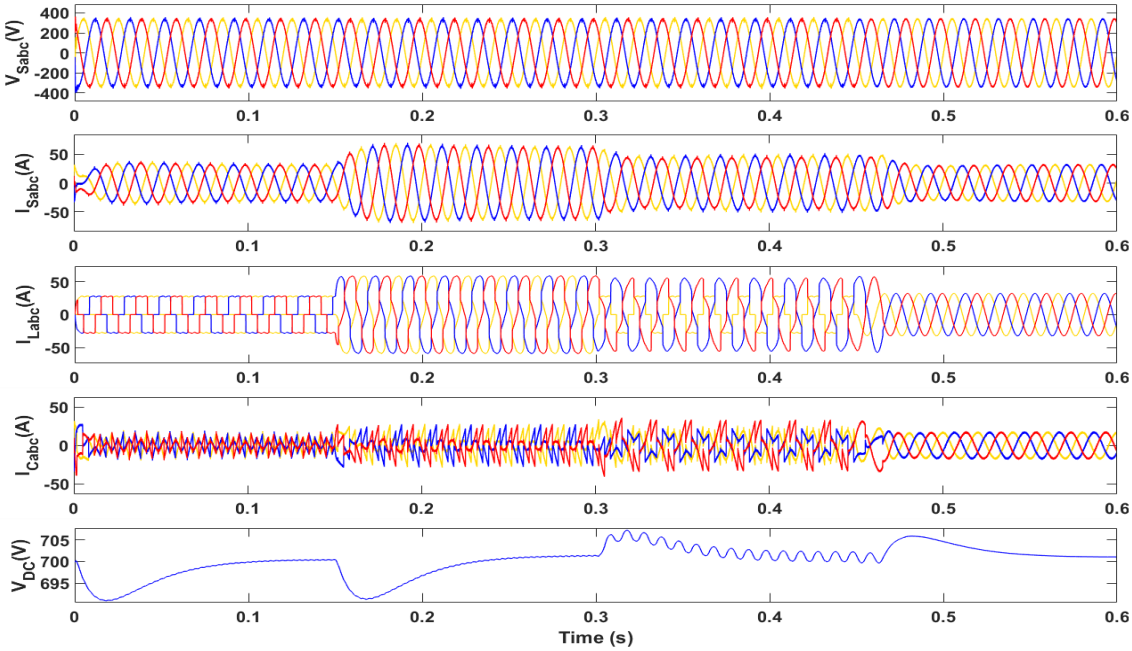

Fig. 3.14. Results for SLMS algorithm

3.4.3 RESULTS FOR SLAD ALGORITHM

Figure 3.15 presents the results of SLAD algorithm. The values of η and α are 0.03 and 0.001 respectively.

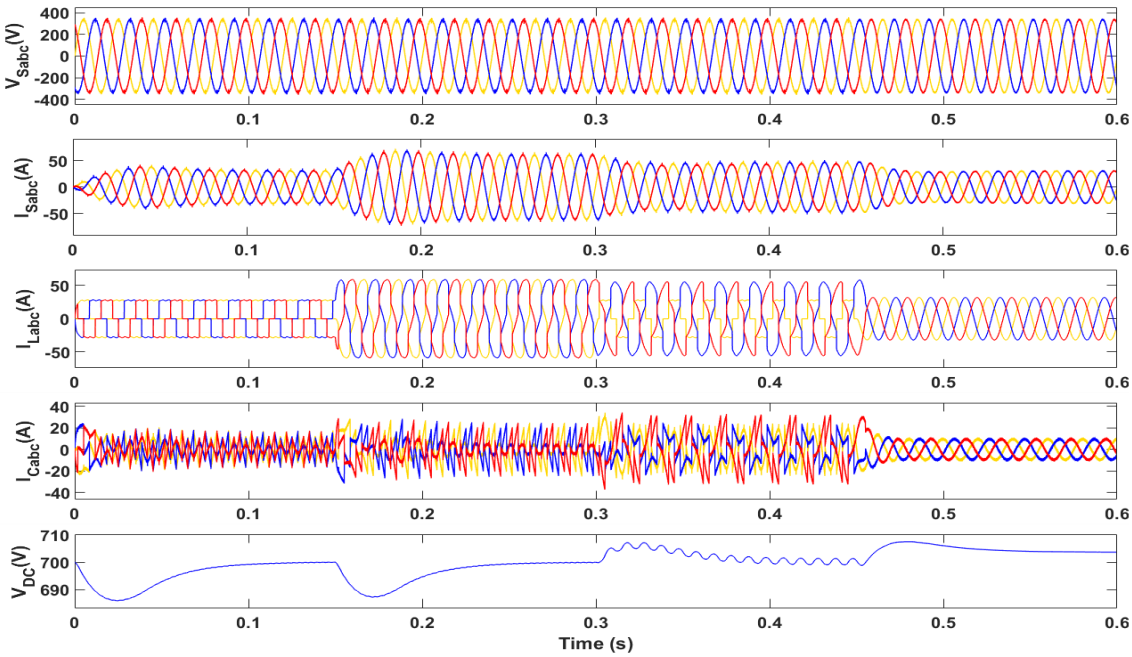

Fig. 3.15. Results for SLAD algorithm

3.4.4 RESULTS FOR SLMF ALGORITHM

Figure 3.16 presents the results of SLMF algorithm. The values of η and α are $2x10^{-5}$ and $5x10^{-6}$ respectively.

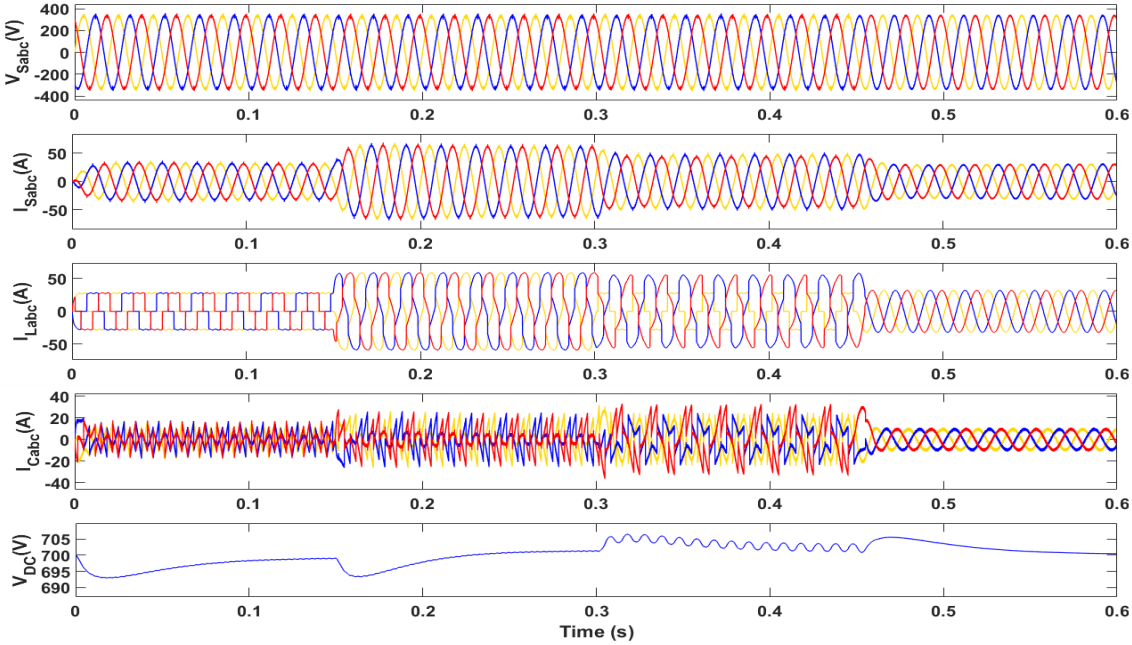

Fig. 3.16. Results for SLMF algorithm

3.4.5 RESULTS FOR SLLAD ALGORITHM

Figure 3.17 presents the results of SLLAD algorithm. The values of α, η and β are 0.001, 0.5 and 0.01 respectively.

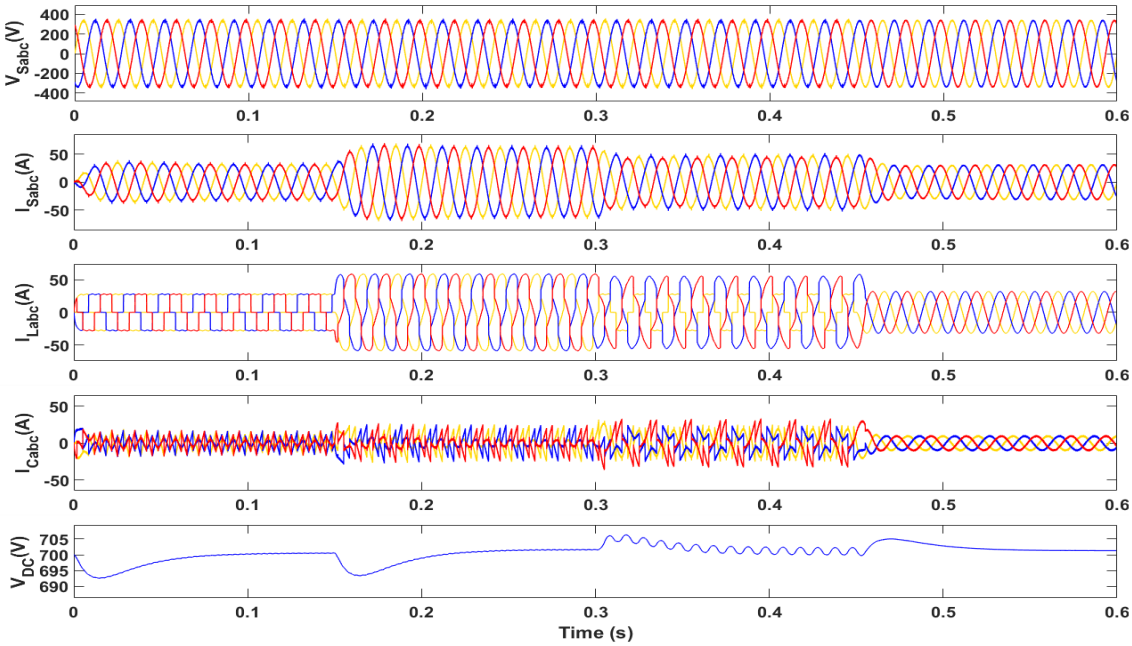

Fig. 3.17. Results for SLLAD algorithm

3.4.6 RESULTS FOR SLMLS ALGORITHM

Figure 3.18 presents the results of SLMLS algorithm. The values of η, α and β are 0.005, 0.001 and 5 respectively.

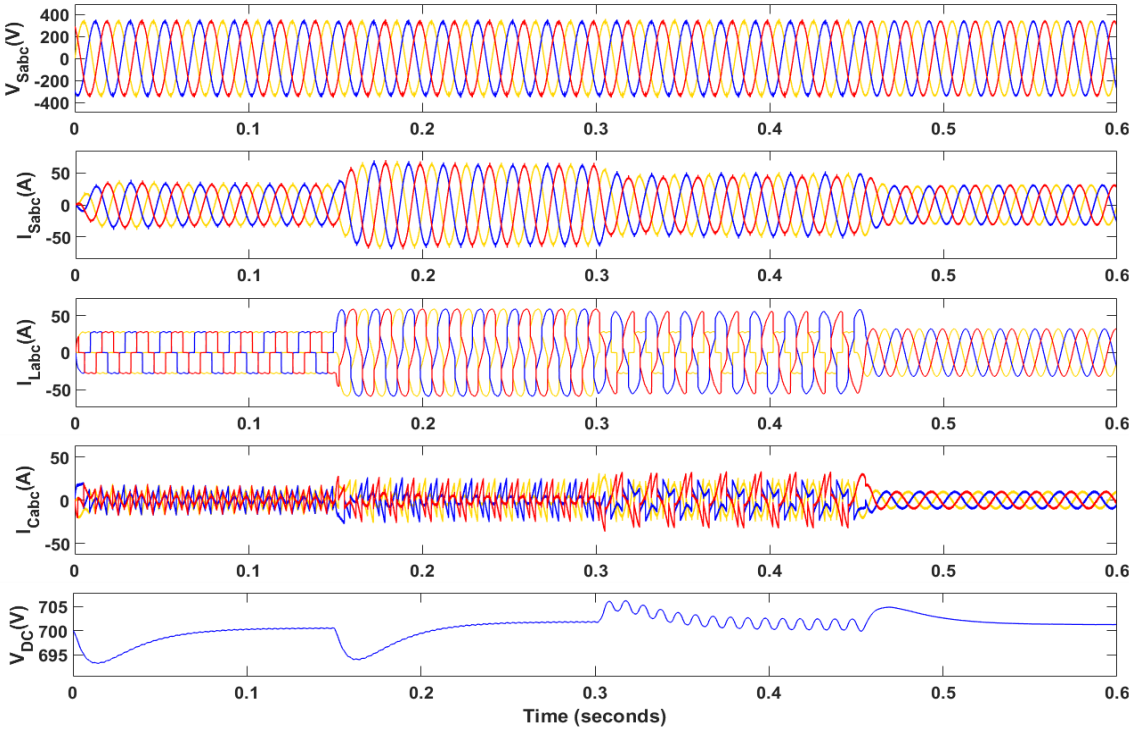

Fig. 3.18. Results for SLMLS algorithm

The source voltage and current waveforms are sinusoidal and in phase at the PCC. Most of the harmonics in the load current are successfully removed by DSTATCOM under different load conditions. The maximum drop and overshoot in DC bus voltage during load change depends on the value of η. With higher values of η the transient response can be made faster with poor steady-state performance. The oscillations in DC bus voltage during unbalanced load condition depends on degree of unbalance and η. With lower value of η the peak to peak magnitude of oscillations is reduced but transient response is slower. The parameter β controls the stiffness of the curve during transient condition.

3.4.7 COMPARISON BETWEEN ADALINE-LMS AND SIGMOID-LMS ALGORITHMS

The performance of Adaline-LMS and sigmoid cost-framework based SLMS algorithm under normal load conditions are similar. Both algorithms eliminate load current's harmonics efficiently. Figure 3.19 presentss weight update comparison of the

two algorithms under normal load conditions. Both algorithm converge to similar steady-state value of load current's fundamental frequency component. The estimated values of load current's fundament direct components are 30, 60, 46 and 31 for non-linear, mix, unbalanced and linear loading conditions respectively. Adaline-LMS converges slightly faster than SLMS for chosen values of η.

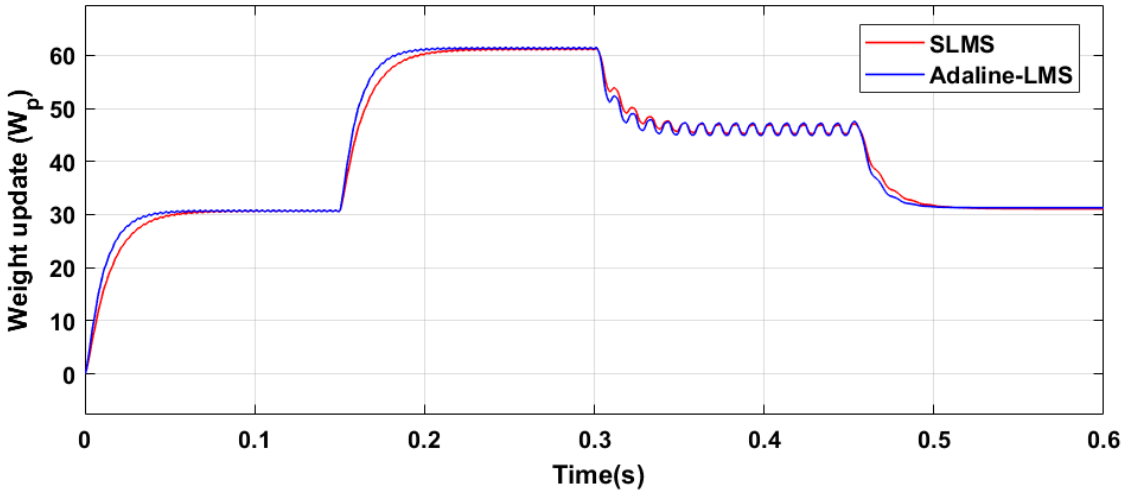

Fig. 3.19. Weight update comparison of Adaline-LMS and SLMS algorithm

As seen in figures 3.20 the voltage of DC-bus settles very close to reference value of 700 V. The voltage of DC-bus drop, during load change, is higher in SLMS than Adaline-LMS for convergence coefficient values 0.001 and 0.003 for Adaline-LMS and SLMS respectively. Though the value of η is higher in SLMS than Adaline-LMS, the convergence is slower due to additional term $S_k(S_k - 1)$. The performance of both the algorithms is similar in these cases.

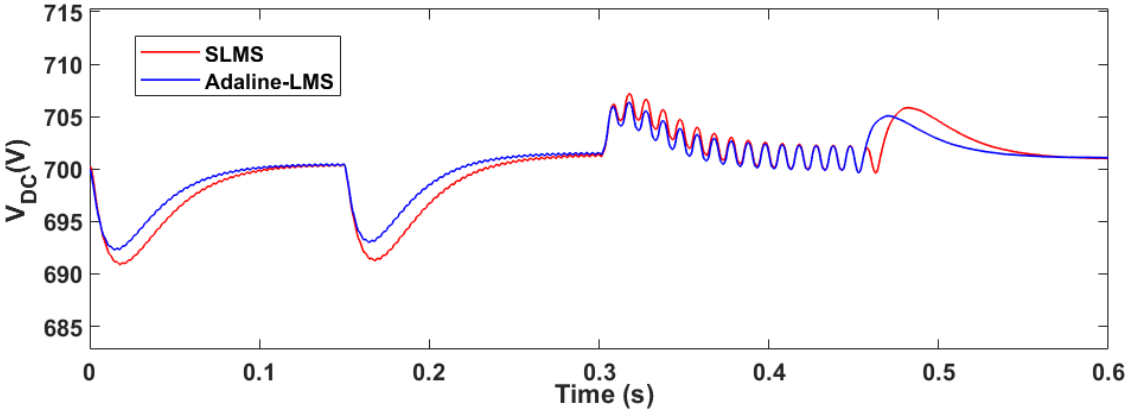

Fig. 3.20. DC bus voltage comparison of Adaline-LMS and SLMS algorithm

For impulsive load condition breaker 1 is kept closed and breaker 3, connecting capacitive load, is closed at 0.1 seconds. Figure 3.21 shows the weight update comparison between Adaline-LMS and SLMS algorithms for this case. In Adaline-LMS

algorithm the weight update, when capacitive load is switched, depends only on the parameter η and error e_k. The rate of rise of weight value is proportional to value of η and e_k. As the load current rises rapidly e_k is very high and the weight value rises rapidly to a peak value of 174. In SLMS algorithm with very high e_k the term $S_k(1-S_k)$ becomes zero and weight update is zero. The parameter α controls the limit of e_k at which the term $S_k(1-S_k)$ tends to zero. Thus, when rate of rise of load current is higher then a set point the weight update is zero in SLMS algorithm.

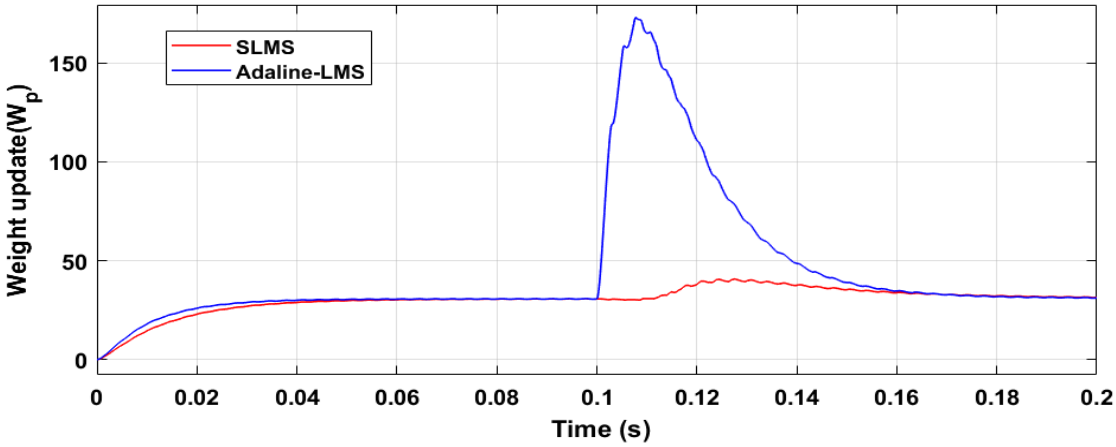

Fig. 3.21. Comparison of Adaline-LMS and SLMS algorithms for impulsive load

The sigmoid based algorithm performs similar to Adaline-LMS algorithm for normal loading conditions. In presence of impulsive load current, the error e_k is so high that the value of S_k is 1 and the value of $S_k(1-S_k)$ becomes zero. This results in zero weight update during impulsive load condition to give more robust performance.

3.4.8 COMPARISON BETWEEN SIGMOID BASED ALGORITHMS

Table 3.1 shows the percentage THD values of source voltage and current for different loading conditions in case of different sigmoid based algorithms.

Time Span (s)	0-0.15		0.15-0.3		0.3-0.45		0.45-0.6	
	Voltage (%)	Current (%)	Voltage (%)	Current (%)	Voltage (%)	Current (%)	Voltage (%)	Current (%)
SLMS	2.06	3.33	2.03	1.75	2.21	3.16	1.47	2.91
SLAD	1.95	3.30	2.10	1.77	2.15	3.10	1.52	2.97
SLMF	1.87	3.19	2.18	1.79	2.12	3.29	1.50	3.02
SLLAD	1.91	3.25	2.17	1.82	2.07	3.52	1.48	2.97
SLMLS	1.94	3.27	2.09	1.78	2.17	3.71	1.53	2.99

Table 3.1. Percentage THD (% of fundamental at 50 Hz) in source voltage and current

The THD values in source voltage are minimum during linear load condition. In source current the THD values are minimum during mix loading condition. For non-linear loading condition the THD values are lowest in SLMF algorithm. For mix loading and linear loading condition SLMS algorithm gives minimum THD. For unbalanced loading SLAD gives minimum THD in current and SLLAD gives minimum THD in voltage. The SLMLS gives moderate THD performance in all loading conditions.

Figure 3.22 shows the weight update comparison for sigmoid based algorithms. The convergence is slowest in SLMS algorithm. The weight update of SLMF algorithm is faster for high value of error e_k but slows down as the error reduces. The weight update curve rises rapidly till around 70 % of steady state value then weight update is very slow. The steady state estimation in SLMF is also lower than other algorithms. The SLLAD algorithm is faster than SLAD but slower than SLMLS. The steady state estimation is same in SLMS, SLLAD, SLAD and SLMLS algorithms.

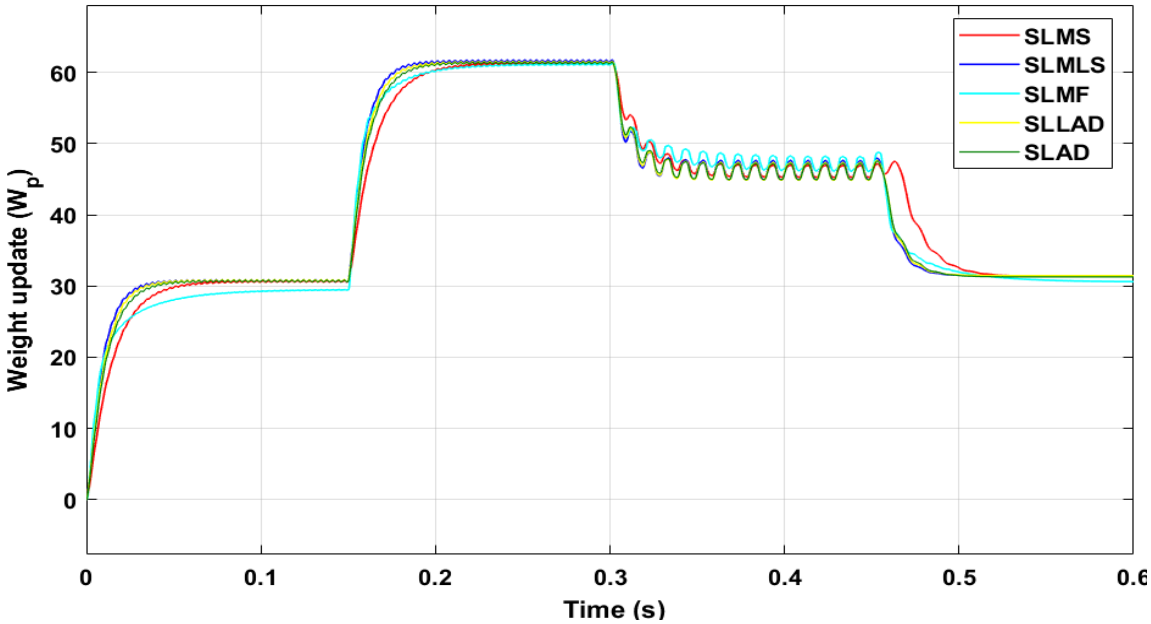

Fig. 3.22. Weight update comparison for sigmoid based algorithms

Figure 3.23 shows the DC bus voltage variations for sigmoid based algorithms. The voltage drop and overshoot are highest in SLAD algorithm and lowest in SLMLS algorithm. In SLAD algorithm during linear load condition DC bus voltage settles much higher than other algorithms. SLMLS and SLLAD algorithms have almost similar DC bus voltage variations. SLMF algorithm converges to steady state value at the lowest speed and during non-linear load condition it settles at a value less than reference value of 700 V.

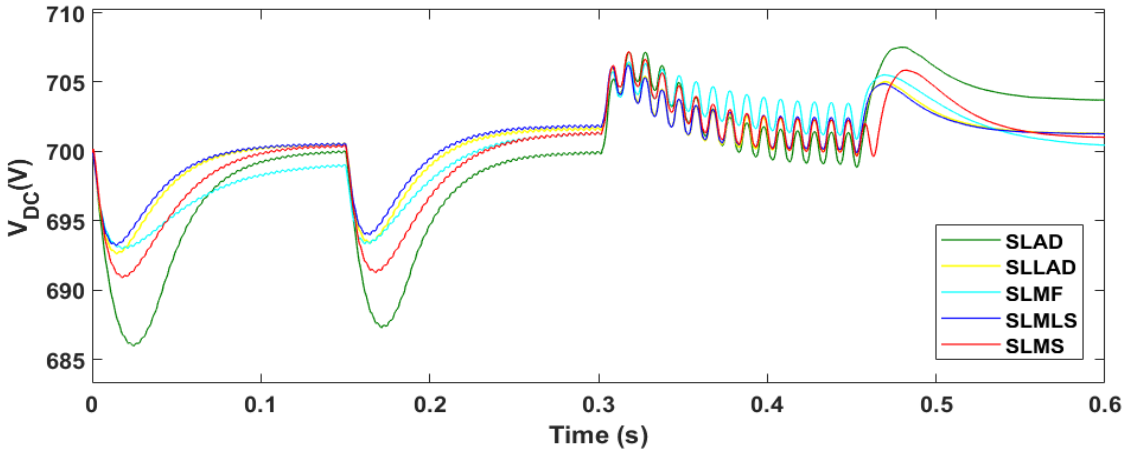

Fig. 3.23. DC bus voltage comparison for sigmoid based algorithm

From the discussion so far, it may be safely deduced that SLMLS algorithm gives best steady state and dynamic performance with faster convergence, stable operation, lower harmonics and accurate estimation. SLMS algorithm is slowest but easiest to implement and gives satisfactory performance.

3.5 CHAPTER SUMMARY

In this chapter sigmoid cost-framework based algorithms are discussed. A three-wire three-phase system is implemented with various non-linear and linear loads. A three-wire DSTATCOM based on voltage source converter is implemented. The Adaline-LMS and sigmoid based algorithms are used for improving power quality in the system. The result presents the effectiveness of algorithm in improving power quality. A comparative study shows that Sigmoid based algorithms gives robust performance in presence of impulsive load condition. The SLMLS algorithm gives better performance in all conditions.

CHAPTER 4

DSTATCOM CONTROL FOR PV-GRID INTEGRATION

Photovoltaic effect is generation of electricity in a material when exposed to photons. Photons are elementary particles that carry solar radiation. The photovoltaic effect was discovered by Edmond Becquerel in 1839. The first device than could generate useful electricity using photovoltaic effect, called photovoltaic cell, were used in satellites in 1960s. The cost of these devices was very high and their application was limited to research. With rising concentration of greenhouse gases in atmosphere and its effects and depleting fossil fuels created an energy and environmental crisis that pushed research for economical and efficient photovoltaic cells for large scale electricity generation [29].

At present use of PV cells for commercial electricity generation is rising rapidly as the cost of installing and maintain a solar power plant is reduced significantly as well as there is a great push from governments and international agencies around the globe for renewable energy generation for sustainable future. Theoretically PV cells have maximum efficiency limit of 33% termeded Shockley-Queisser limit. Commercially available PV modules have efficiency around 20%. Research is going on in field of multi-junction cells to achieve maximum theoretical efficiency of around 50%.

4.1 CHARACTERISTICS OF PV MODULES

In practical conditions solar radiation varies with various factors such as geography, weather, temperature, dust etc. Hence the output of PV modules varies depending on these conditions. The solar radiation at earth's surface is different at different geographical locations. The temperature varies with different atmospheric conditions. Temperature and Solar irradiance are quantifiable to represent the performance of PV module in different conditions. Figure 4.1 and 4.2 presents the changes in PV output with different levels of irradiance and temperatures.

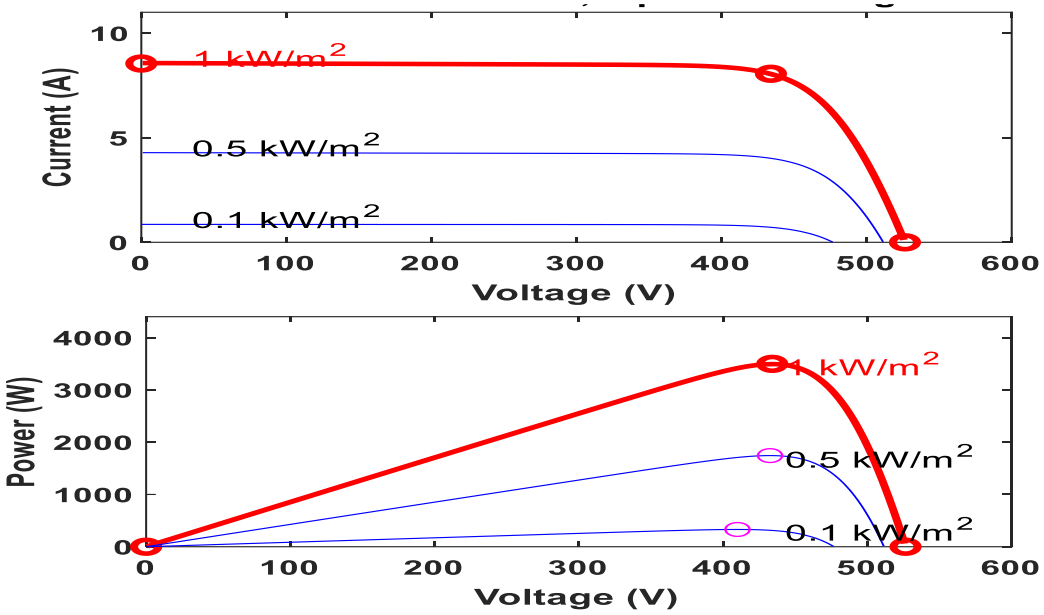

Fig. 4.1. P-V and I-V curve for different irradiance levels of PV

Figure 4.1 shows typical voltage versus power and voltage versus current curve for irradiance levels of 1 kW/m^2, 500 W/m^2 and 100 W/m^2. The current output of PV panel remains same for a large range of voltage values then decrease rapidly. The current and power decreases with decreasing irradiance levels. Figure 4.2 shows typical voltage versus power and voltage versus current curve with values of temperature as 100 °C, 45°C and 25°C. With increase in temperature the voltage, at which current starts decreasing rapidly, decreases and the maximum power that can be generated by PV panel also decreases.

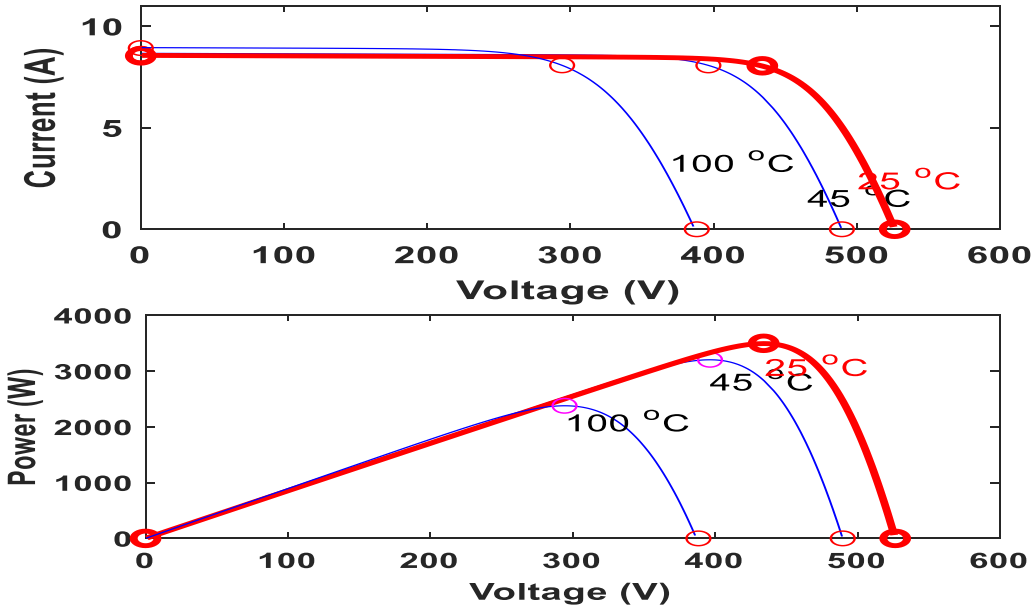

Fig. 4.2. P-V and I-V curve for different temperature levels of PV

4.2 SYSTEM DESIGN AND MATLAB MODELLING

For integration of PV system with existing AC grid system a constant DC voltage is required to be maintained at all irradiance and temperature levels. There are several control strategies proposed in research works. Fig. 4.3 presents the DSTATCOM's configuration for PV-Grid integration in a three-wire three-phase distribution system. The circuit shown in figure 4.3 requires two stage control. In first stage Maximum Power Point Tracking (MPPT) algorithm is utilised to extract maximum available power and maintain constant DC voltage by controlling duty ratio of DC to DC converter and in second stage DSTATCOM control is implemented to supply active power at the PCC.

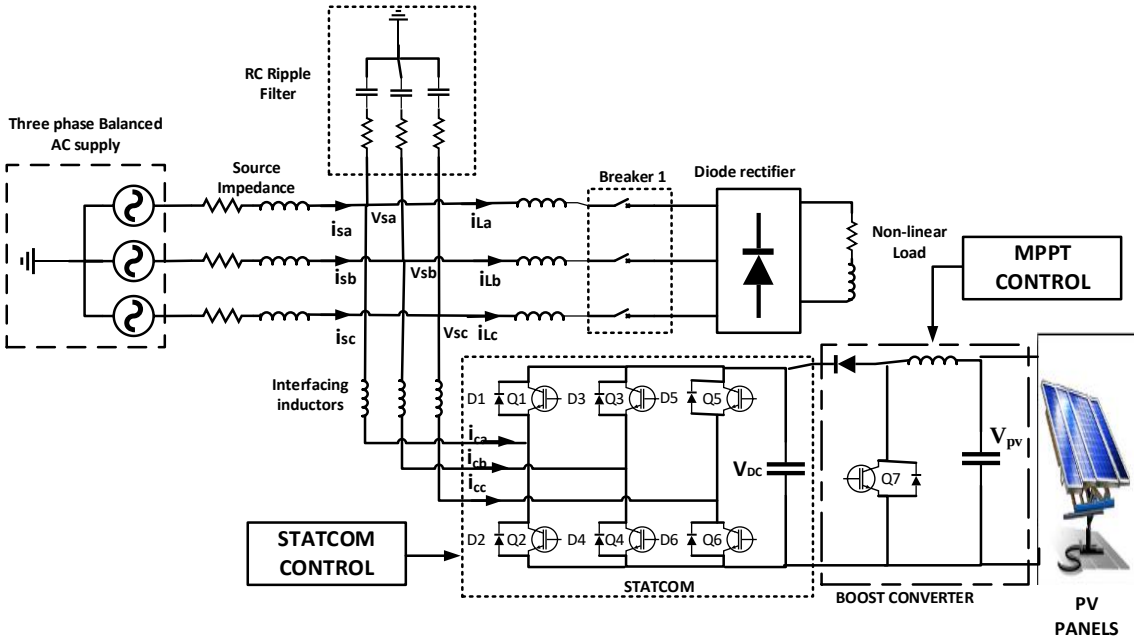

Fig. 4.3 STATCOM for PV-Grid integration

The design of AC source, load and DSTATCOM is discussed in previous chapter. The supply system voltage at distribution level is 415 V line-to-line. The system frequency is chosen as 50 Hz. The value of resistance, inductance and capacitance of series RLC branch of source impedance is selected as 0.1 Ω, 1 mH and 0 F. A non linear load is implemented using a resistive-inductive load at the DC side of diode rectifier. For 415 V line-to-line voltage of AC system the reference value of DC capacitor voltage is selected as 700 V. The DC bus capacitor value C_{DC} is chosen as 15000 μF. The value of interfacing inductors is selected as 2 mH. The capacitor of ripple filter is designed as C_f = 10 μF with resistance R_f of 5 Ω in series. The value of smoothing reactor on load side is 2 mH.

4.2.1 DESIGN AND IMPLEMENTATION OF PV SYSTEM

MATLAB/Simulink library has built-in 'PV array block' that represents photovoltaic module's array. The array consists of parallel strings and each string consist of series PV modules. The number of parallel strings and series modules are modifiable as required. There are a number of preset PV module designs, as per National Renewable Energy Laboratory (NREL) System Advisor Model (Jan. 2014), are available to choose from. Figure 4.4 gives an equivalent circuit representation of PV array with a diode, light generated current source I_L, series (R_s) and shunt resistors (R_{sh}).

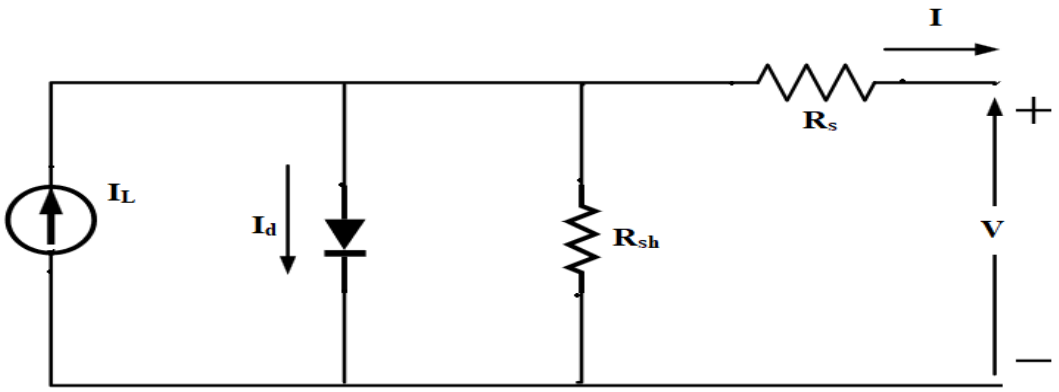

Fig. 4.4. Equivalent circuit representation of PV array

For this study an array of 10 series connected modules in each of the 8 parallel strings is used. Each module has 60 PV cells. The module's Short Circuit Current I_{sc} and Open Circuit Voltage V_{oc} ratings are 8.55 A and 37.5 V respectively. The current and voltage value for Peak power output in each module is 8.06 A and 31 V respectively.

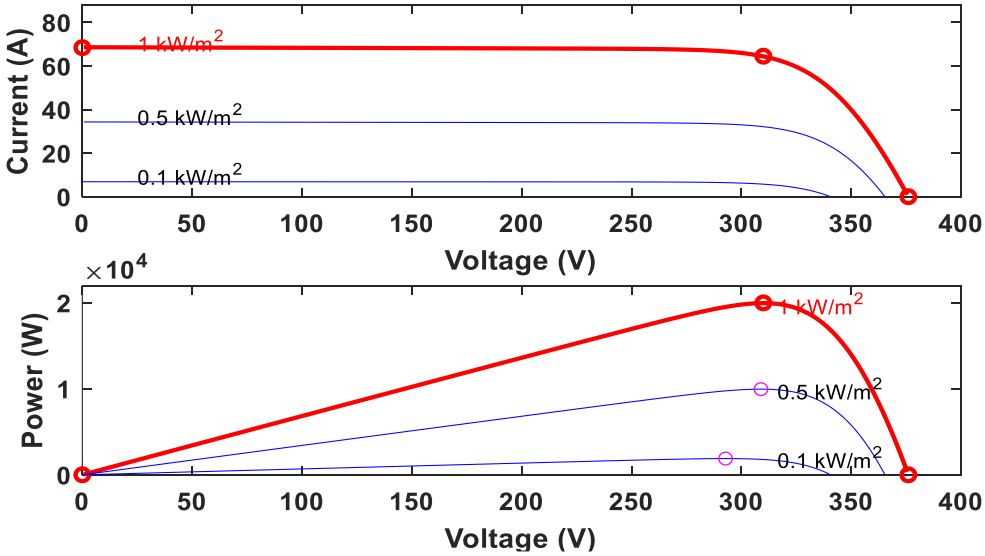

Fig. 4.5. P-V and I-V characteristics of PV array at 25 °C

Figure 4.5 presents the characteristics of selected PV array. The maximum power at irradiance level 1000 W/m^2 is around 20 kW. The current and voltage at point of peak power is around 60 A and 315 V respectively.

4.2.2 BOOST CONVERTER DESIGN AND IMPLEMENTATION

A boost converter increases the voltage level to its output from its input. This is achieved using an energy storing element (inductor) and switching devices. The circuit diagram of boost converter is given in figure 4.3. It comprises of an inductor, an IGBT with antiparallel diode and a diode at output. When the IGBT is ON the inductor stores energy and when the IGBT is OFF inductor work as second source in series with source voltage causing higher voltage to charge output capacitor through diode. The inductor rating and switching frequency are chosen such that inductor will not fully discharge between charging stages. The duty cycle of boost converter is given as:

$$D = 1 - \frac{V_i}{V_o} \tag{4.1}$$

Here V_o and V_i are output and input voltages of boost converter respectively. For this design the output voltage is fix at 700 V and input voltage varies with PV array output. The value of capacitor on the PV side is calculated as:

$$C = \frac{4V_{mp}D_{mp}}{\Delta V_i R_i f_s} \tag{4.2}$$

Here V_{mp} and D_{mp} are input voltage and duty cycle at maximum power point with values 315 V and 0.55. ΔV_i is ripple in input voltage taken as 2% of V_i, 6.3. R_i is input resistance calculated using $R_o(1 - D^2)$ and f_s is switching frequency is 5000 Hz. $R_o = 2.5 \times (V_{mp}/I_{mp})$ = 13.125 Ω. R_i is found to be 43.38 Ω. The input capacitor value is calculated as $C = (4 \times 315 \times 0.55)/(6.3 \times 43.38 \times 5000) = 507.15\ \mu F$. The input capacitor is chosen as 500 μF.

The inductor value is calculated as:

$$L = \frac{V_{mp}D_{mp}}{2\Delta I_o f_s} \tag{4.3}$$

Here ΔI_o is current ripples taken as 4 % of I_{mp}, 2.4 A. the value of inductor is calculated as $L = (315 \times 0.55)/(2 \times 2.4 \times 5000) = 7.22\ mH$. The inductor value is taken as 10 mH.

4.3 CONTROLLING THE PV-DSTATCOM SYSTEM

The control for PV-DSTATCOM system is a two-stage control. In first stage Maximum Power Point Tracking (MPPT) control is implemented using method of incremental conductance which changes the duty ratio of IGBT to track maximum power point.

4.3.1 METHOD OF INCREMENTAL CONDUCTANCE

Method of incremental conductance is used for tracking the voltage at which maximum power can be generated by the PV system. From figures 4.1 and 4.2 we can see that the slope of voltage versus power curve is zero at the point of highest power level.

$$\frac{dP}{dV} = 0 \tag{4.4}$$

Putting $P = I \times V$ in 4.4 we get $I + V\frac{dI}{dV} = 0$ (4.5)

By rewriting (4.5), the following equation is obtained:

$$\frac{dI}{dV} = -\frac{I}{V} \tag{4.6}$$

Here I/V is called instantaneous conductance and dI/dV is called incremental conductance. Hence by minimizing the error between dI/dV and $-I/V$ MPP is achieved. The output current I_{pv} and voltage V_{pv} of PV arrays are measured and used as feedback signals for this control algorithm. For minimizing the error integral controller is used. The output of controller is change in duty ratio which is subtracted from initial value of duty ratio to obtain correct duty ratio for Pulse Width Modulation (PWM) control of boost converter's IGBT. The initial value of duty ratio is chosen as 0.5. A PWM Generator block is implemented for producing gate signal of IGBT. The inputs to this block are duty ratio and switching frequency. Figure 4.6 gives the MATLAB implementation for incremental conductance algorithm.

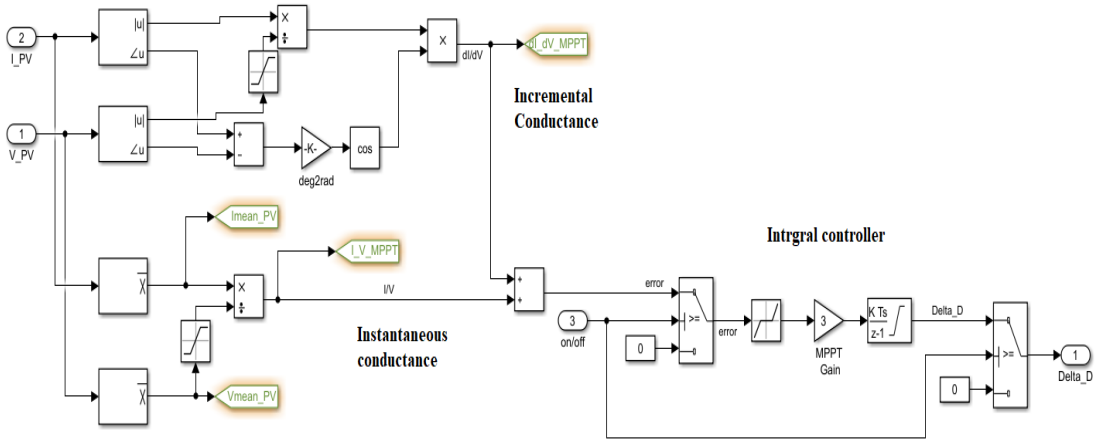

Fig. 4.6. MATLAB implementation of incremental conductance algorithm

4.3.2 DSTATCOM CONTROL WITH SLMLS ALGORITHM

Integration of PV with AC system requires little modification in the DSTATCOM control algorithm described in section 2.5.1 and 3.1.5. The equivalent value of current generated by PV in AC side can be written as

$$I_{ac} = \frac{2}{3}\left(\frac{V_{pv}I_{pv}}{V_{AC}}\right) \tag{4.7}$$

The direct component of reference current obtained by equation 2.12 can be modified as

$$i_p = W_p + i_{lDC} - I_{ac} \tag{4.8}$$

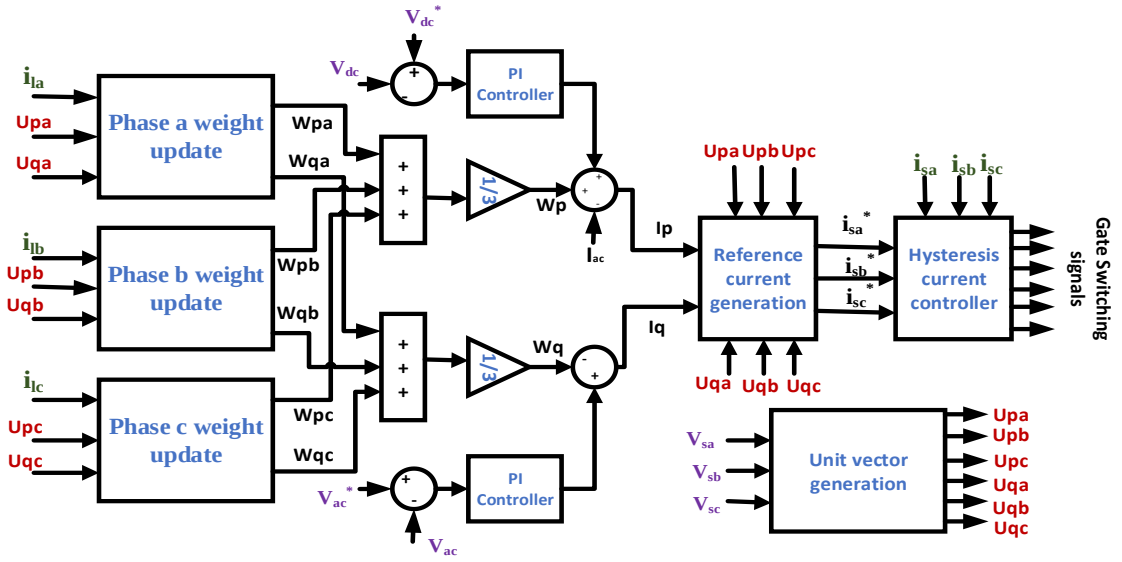

Fig. 4.7. DSTATCOM control for PV integrated system

Other steps in the DSTATCOM control algorithm remains same as in section 2.5.1. The modified block diagram of control algorithm is given in figure 4.7.

4.4 SIMULATION RESULTS AND DISCUSSION

The simulation of proposed system is performed in MATLAB/Simulink for various irradiance levels. In powergui block simulation type is set to discrete and sample time is selected as 5e-6. The value of resistor and inductor connected at the output of diode rectifier are 10 Ω and 50 mH respectively. The temperature input to PV array is set to 25 °C and the irradiance is varied using a stair generator block. The circuit breaker is closed at 0 seconds. From 0 to 0.08 seconds the irradiance level is zero. At 0.08 seconds the irradiance level rises to 500 W/m^2. From 0.25 seconds the irradiance level changes to 1000W/m^2. At 0.55 seconds the irradiance level reduces from 1000 W/m^2 to 700 W/m^2. At 0.8 seconds the irradiance level changes from 700 W/m^2 to 400 W/m^2. Figure 4.8 shows the source voltage (phase to ground) V_{Sabc}, current I_{Sabc}, load current I_{Labc}, DSTATCOM current I_{Cabc} and DC bus voltage V_{DC} and irradiance level I_r for SLMLS algorithm. The values of η, α and β are 0.005, 0.001 and 5 respectively.

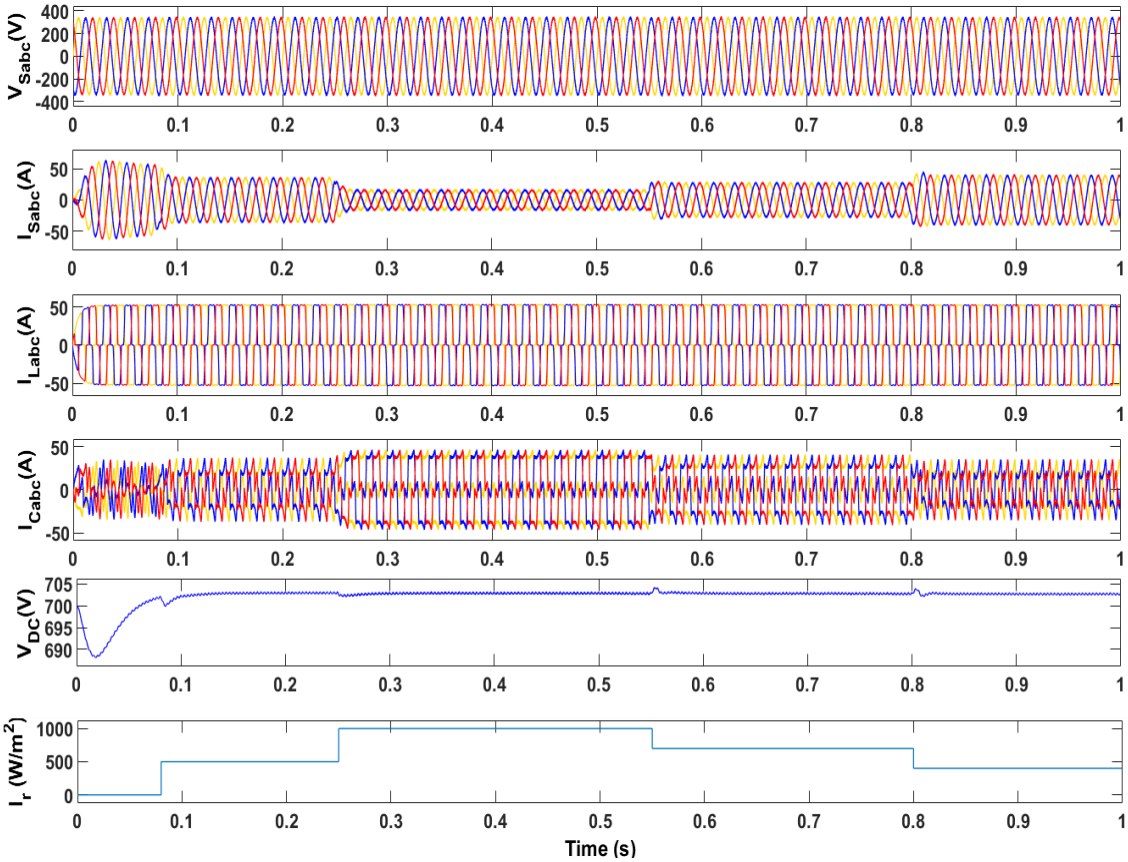

Fig. 4.8. Results for PV integrated system

4.4.1 PERFORMANCE OF DSTATCOM

As seen in figure 4.8 the load current is not sinusoidal. The THD in load current is around 20.72% with magnitude of fundament component 57.63 A. The DSTATCOM successfully eliminates harmonics present in load current and source current is almost sinusoidal in all cases of irradiance levels. The DC capacitor voltage settles at reference of 700 V. The THD in source voltage considering harmonics of order up to 100 is below 1.5%. Figure 4.9 shows harmonic spectra of source current at 0.05 second. The irradiance level is zero at this time and power supplied by PV system is zero. The load's active power is fully supplied by the three phase source. The magnitude of source current's fundamental component is 57.06 A. The THD value considering harmonics of order up to 100 is 1.08%.

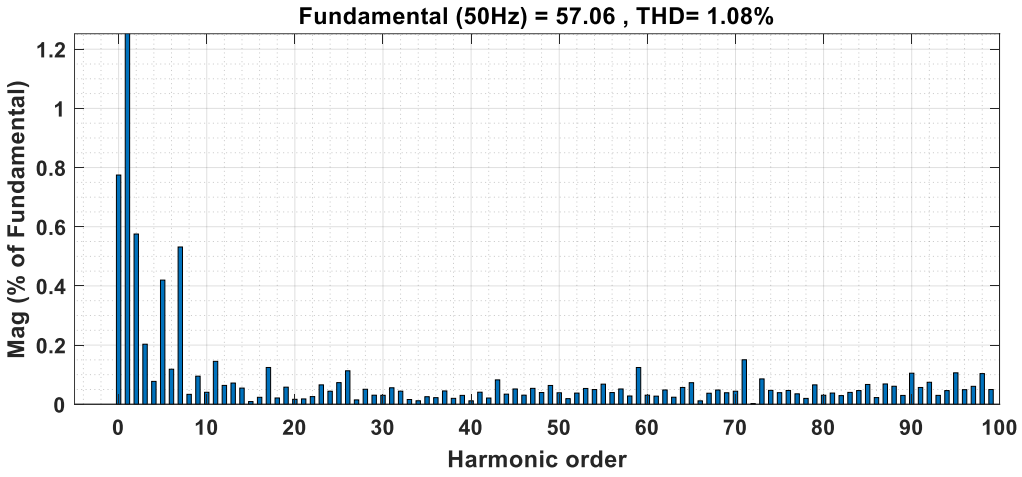

Fig. 4.9. Source current's harmonic spectra at 0.05 seconds

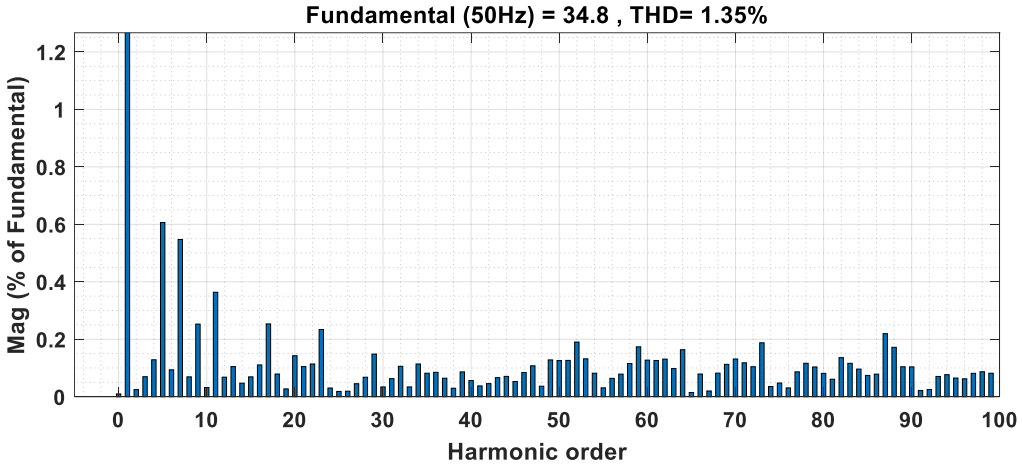

Fig. 4.10. Source current's harmonic spectra at 0.15 seconds

Figure 4.10 shows harmonic spectra of source current at 0.15 second. The irradiance level at this time is 500 W/m^2. The load is fed from both the three phase source and PV system. The magnitude of source current's fundamental component is 34.8 A. The THD value considering harmonics of order up to 100 is 1.35%.

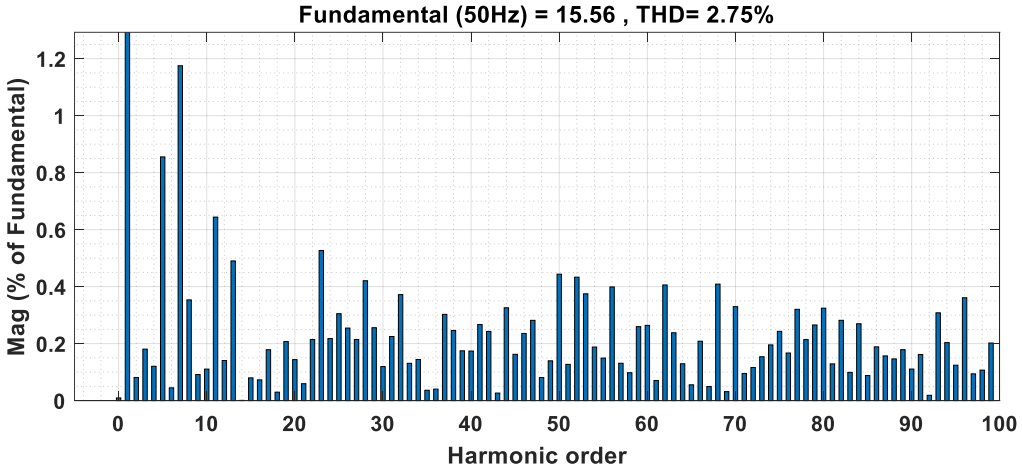

Fig. 4.11. Source current's harmonic spectra at 0.4 seconds

Figure 4.11 shows source current's harmonic spectra at 0.4 seconds. At this time the irradiance level is 1000 W/m^2. The load is supplied by the three phase source and the PV system. The magnitude of source current's fundamental component is 15.56 A. The THD value considering harmonics of order up to 100 is 2.75%. Figure 4.12 shows harmonic spectra of source current at 0.7 seconds. The irradiance level is 700W/m^2 at this time. The magnitude of source current's fundamental component is 26.88 A. The THD value considering harmonics of order up to 100 is 1.82%.

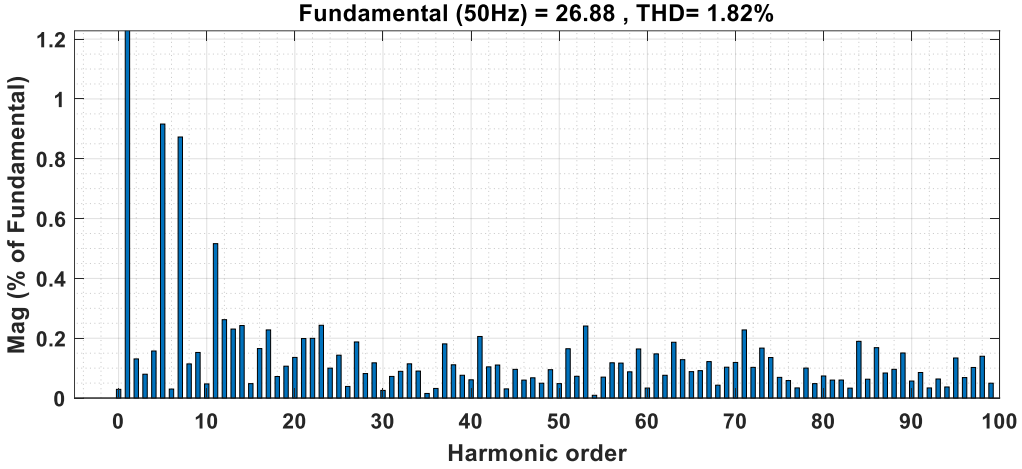

Fig. 4.12. Source current's harmonic spectra at 0.7 seconds

Figure 4.13 shows source current's harmonic spectra at 0.9 seconds. The irradiance level is 400W/m^2 at this time. The magnitude of source current's fundamental

component is 38.71 A. The THD value considering harmonics of order up to 100 is 1.33%.

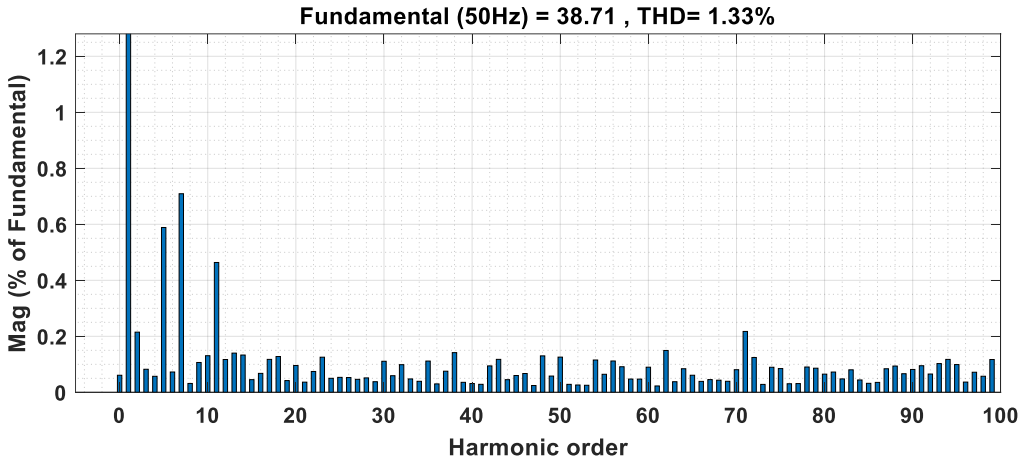

Fig. 4.13. Source current's harmonic spectra at 0.9 seconds

The THD in source current rises as it's magnitude is close to zero. This is caused by ripples in DC capacitor voltage and switching losses in the DSTATCOM whose effects is dominant as current magnitude tends close to zero. The source current and voltage THD are within limits prescribed in IEEE standards 1547-2018 [7]. The magnitude of maximum current supplied by PV system is around 40 A at irradiance level 1000 W/m^2.

4.4.2 PERFORMANCE OF INCREMENTAL CONDUCTANCE ALGORITHM

Figure 4.14 presents the current (I_{pv}) and voltage (V_{pv}) at the terminals of the PV array. The initial capacitor voltage is set to 300 V at the start of simulation.

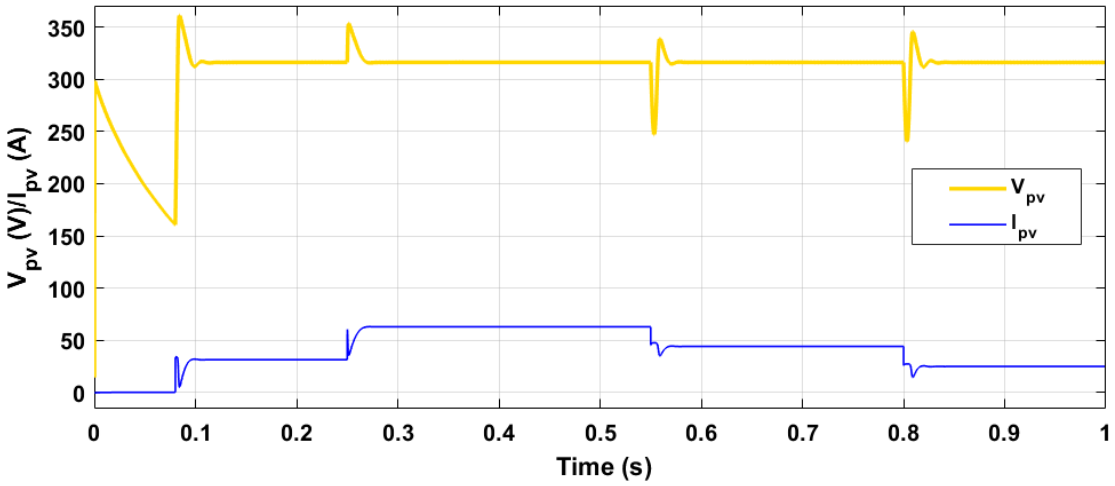

Fig. 4.14. PV array terminal current and voltage

As shown in figure 4.14 the voltage at the terminals of PV array is maintained at a constant value of around 316 V and current varies with different irradiance levels. The current values are 31 A, 62 A, 44 A and 25 A for 500 W/m^2, 1000 W/m^2, 700 W/m^2 and 400 W/m^2 respectively. The current and voltage values are very close to the values shown in figure 4.5 (I-V and P-V characteristics of PV array at 25 °C). The voltage and current settles to steady state value within 0.04 second. The Incremental conductance MPPT algorithm efficiently tracks maximum power point with fast transient response.

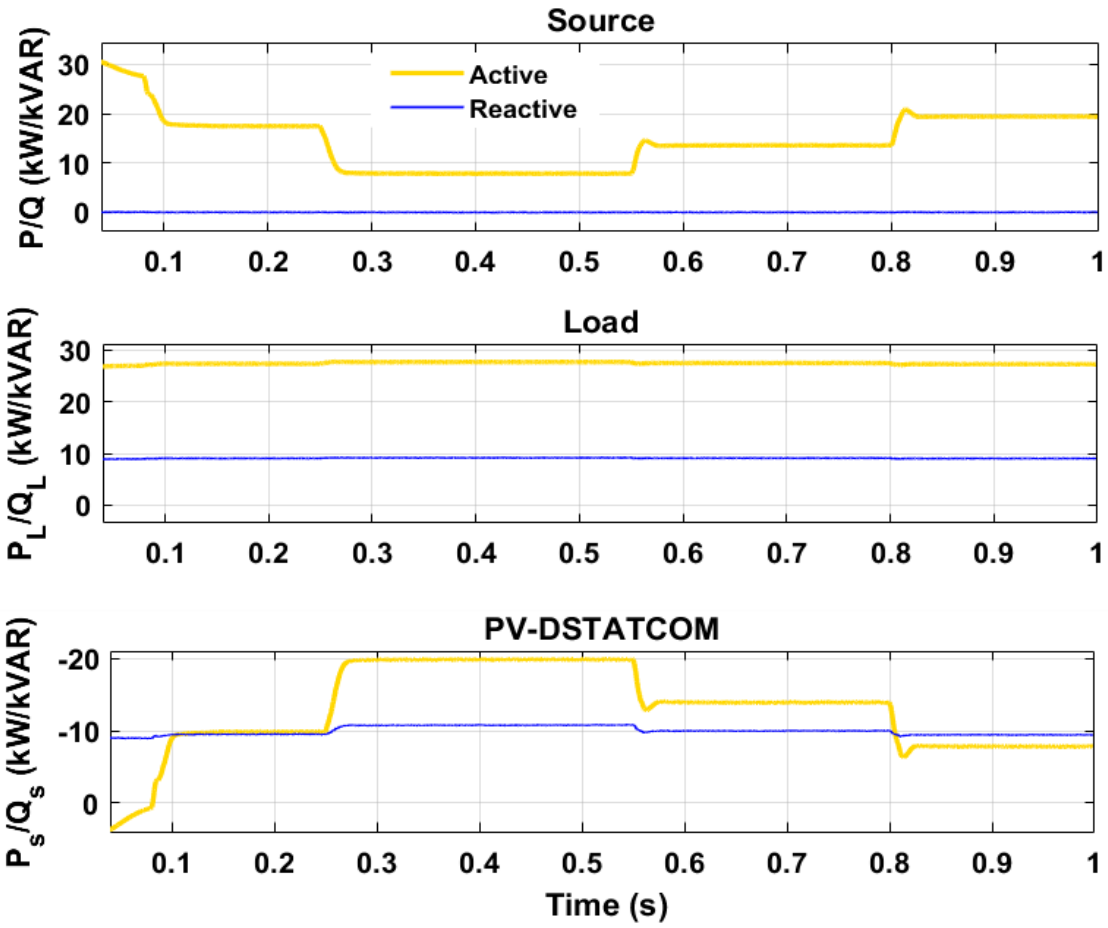

Fig. 4.15. Instantaneous reactive and active power

Fig. 4.15 presents the instantaneous reactive and active power variations of source (P/Q), load (P_L/Q_L) and PV-DSTATCOM (P_s/Q_s). The load consumes around 27 kW active and 9 kW reactive power. The DSTATCOM supplies all the reactive power requirement of the load and reactive power supplied by source side at PCC is zero. At 0.08 s PV-DSTATCOM starts supplying active power and power supplied by source reduces to 17.5 kW from 27 kW. PV-STATCOM supplies 10 kW power at 500 W/m2 irradiance level. At 0.25 s irradiance level changes to maximum of 1000 W/m2. The PV-STATCOM supplies 20 kW active power and active power supplied by source reduces

to 8 kW. The maximum power supplied by PV-STATCOM is close to value of maximum power shown in Fig. 4.5. At 0.55 s and 0.8 s irradiance levels decreases to 700 W/m^2 and 400 W/m^2 respectively and drop in power supplied by PV-STATCOM is observed.

4.5 CHAPTER SUMMARY

In this chapter a brief introduction to PV electricity generation is given. Characteristics and design of a PV array is presented. A boost converter is implemented to step up PV array output voltage. Incremental Conductance method is discussed and implemented for MPPT control of boost converter. A PV-DSTATCOM system with SLMLS control algorithm is presented and results are analysed.

CHAPTER 5

CONCLUSIONS AND FUTURE SCOPE

In this work different power quality issues because of increased use of non-linear load and rising penetration of renewable energy resources in grid connected system are addressed. An implementation of DSTATCOM as Shunt Active Power Filter for improving power quality in three-wire three-phase distribution system is presented. A PV-grid integration using DSTATCOM is also presented. Various control algorithms for control of DSTATCOM as Shunt Active Power Filter are reviewed. Adaline-LMS and sigmoid cost framework based SLMS, SLMF, SLAD, SLLAD and SLMLS algorithms for DSTATCOM control are analysed in software MATLAB/Simulink.

All the algorithms are efficient in successfully removing harmonics in the load current under different load condition and the THD in source current and voltage are within limits as per IEEE 519-2014 standards. The maximum overshoot and drop in DC bus voltage at the time of load change depends on the value of convergence coefficient (η). With higher values of η the transient response can be made faster at the expense of steady state performance. There are oscillations of variable magnitude present in DC bus voltage during unbalanced load conditions. These oscillations depend on degree of unbalance and η. With lower value of η the peak to peak magnitude of oscillations can be reduced but transient response is slower. The parameter β in logarithmic based algorithms controls the stiffness of the curve during transient condition. The sigmoid based algorithm performs similar to Adaline-LMS algorithm for normal loading conditions. In presence of impulsive load current, the error e_k is so high that the value of S_k is 1 and the value of $S_k(1 - S_k)$ becomes zero. This results in zero weight update during impulsive load condition to give more robust performance. SLMS algorithm is slowest but easiest to implement and gives satisfactory performance. SLMLS algorithm gives best steady state and dynamic performance with faster convergence, stable operation, lower harmonics and accurate estimation.

The SLMLS algorithm and Incremental conductance algorithm are implemented for control of DSTATCOM and boost converter of PV-DSTATCOM system. The THD in source current rises as it's magnitude is close to zero. This is caused by ripples in DC capacitor voltage and switching loss in the DSTATCOM whose effects is dominant as current magnitude tends close to zero. The THD of source current and voltage are within limits prescribed in IEEE standards 1547-2018. The Incremental conductance MPPT algorithm efficiently tracks maximum power point with fast transient response and maintains constant voltage at output terminals of PV array. The PV-DSTATCOM system eliminates harmonics present in load current and supplies active power to load generated by the PV system.

In this work software simulations of DSTATCOM for power quality improvement and PV-grid integration are presented. An experimental hardware setup of above system can be implemented and results can be verified for future work. A two-stage control for PV-STATCOM is presented in this work. A single stage control can be developed and implemented for reducing cost. Other advanced MPPT algorithms like Particle Swarm Optimization (PSO), Discrete time ripple correlation control etc. can be implemented for boost converter control.

REFERENCES

[1] Narain G. Hingorani and L. Gyugyi, “Understanding FACTS: Concepts and Technology of Flexible ac transmission system” IEEE Press, 2000.

[2] Prabha Kundur, “Power System Stability and Control” 1994 McGraw-Hill, Inc.

[3] R. Mohan Mathur and Rajiv K. Varma, “Thyristor-Based FACTS Controllers for Electrical Transmission Systems” 2002 John Wiley and Sons, Inc.

[4] Bhim Singh, Ambrish Chandra and Kamal Al-Haddad, “Power quality problems and mitigation techniques” 2015 John Wiley and Sons Ltd.

[5] Suman Bhowmick, “Flexible AC Transmission Systems (FACTS): Newton Power-Flow Modeling of Voltage-Sourced Converter-Based Controllers” 2016 CRC press.

[6] IEEE Recommended Practice and Requirements for Harmonic Control in Electric Power Systems," in IEEE Std 519-2014 (Revision of IEEE Std 519-1992) , pp.1-29, June 11 2014. doi: 10.1109/IEEESTD.2014.6826459.

[7] IEEE Standard for Interconnection and Interoperability of Distributed Energy Resources with Associated Electric Power Systems Interfaces," in IEEE Std 1547-2018 (Revision of IEEE Std 1547-2003) , vol., no., pp.1-138, April 6 2018. doi: 10.1109/IEEESTD.2018.8332112.

[8] D. Kumar and Rajesh, "Modelling, Analysis and Performance of a DSTATCOM for Unbalanced and Non-Linear Load," 2005 IEEE/PES Transmission & Distribution Conference & Exposition: Asia and Pacific, Dalian, 2005, pp. 1-6. doi: 10.1109/TDC.2005.1547142.

[9] R. Panigrahi, P. C. Panda and B. D. Subudhi, "Comparison of performances of hysteresis and dead beat controllers in active power filtering," 2012 IEEE Third International Conference on Sustainable Energy Technologies (ICSET), Kathmandu, 2012, pp. 287- 292. doi: 10.1109/ICSET.2012.6357413.

[10] C. Kumar and M. K. Mishra, "A Voltage-Controlled DSTATCOM for Power-Quality Improvement," in IEEE Transactions on Power Delivery, vol. 29, no. 3, pp. 1499-1507, June 2014. doi: 10.1109/TPWRD.2014.2310234.

[11] B. Singh, P. Jayaprakash and D. P. Kothari, "Isolated H-bridge VSC Based 3-phase 4- wire DSTATCOM for power quality improvement," 2008 IEEE International Conference on Sustainable Energy Technologies, Singapore, 2008, pp. 366-371. doi: 10.1109/ICSET.2008.4747034

[12] S. Kumar, B. Singh, "Control of 3 Leg VSC Based 3Phase 4Wire DSTATCOM using Modified Instantaneous Symmetrical Component Theory," in International Journal of Automation and Power Engineering (IJAPE) Vol. 2 No. 6, September 2013

[13] S. Kumar and B. Singh, "Control of 4-Leg VSC based DSTATCOM using modified Instantaneous Symmetrical Component Theory," 2009 International Conference on Power Systems, Kharagpur, 2009, pp. 1-6. doi: 10.1109/ICPWS.2009.5442769.

[14] A. Dheepanchakkravarthy, Jebasalma, “A Modern Approach of a Three Phase Four Wire Dstatcom for Power Quality Improvement Using T Connected Transformer”, in International Journal of Engineering Inventions, Vol. 1, No. 4 pp: 80-90, 2012.

[15] B. Singh, P. Jayaprakash and D. P. Kothari, "A T-Connected Transformer and Three-leg VSC Based DSTATCOM for Power Quality Improvement," in IEEE Transactions on Power Electronics, vol. 23, no. 6, pp. 2710-2718, Nov. 2008. doi: 10.1109/TPEL.2008.2004273.

[16] P. Jayaprakash, B. Singh and D. P. Kothari, "Implementation of an Isolated Three-Leg VSC with Star/Hexagon Transformer Based Three-Phase Four-Wire DSTATCOM," 2009 Second International Conference on Emerging Trends in Engineering & Technology, Nagpur, 2009, pp. 533-538. doi: 10.1109/ICETET.2009.122.

[17] B. N. Singh, B. Singh, A. Chandra and K. Al-Haddad, "Design and digital implementation of active filter with power balance theory," in IEEE Proceedings - Electric Power Applications, vol. 152, no. 5, pp. 1149-1160, 9 Sept. 2005. doi: 10.1049/ip- epa:20050097.

[18] B. Singh and S. Kumar, "Control of DSTATCOM using IcosΦ algorithm," 2009 35th Annual Conference of IEEE Industrial Electronics, Porto, 2009, pp. 322-327. doi: 10.1109/IECON.2009.5414942

[19] M. Labeeb and B. S. Lathika, "Design and analysis of DSTATCOM using SRFT and ANN-fuzzy based control for power quality improvement," 2011 IEEE Recent Advances in Intelligent Computational Systems, Trivandrum, 2011, pp. 274-279. doi: 10.1109/RAICS.2011.6069317.

[20] B. Singh and S. R. Arya, "Implementation of Single-Phase Enhanced Phase-Locked Loop-Based Control Algorithm for Three-Phase DSTATCOM," in IEEE Transactions on Power Delivery, vol. 28, no. 3, pp. 1516-1524, July 2013. doi: 10.1109/TPWRD.2013.2257876

[21] A. Singh, M. Badoni and B. Singh, "Application of least means square algorithm to shunt compensator: An experimental investigation," 2014 IEEE International Conference on Power Electronics, Drives and Energy Systems (PEDES), Mumbai, 2014, pp. 1-6. doi: 10.1109/PEDES.2014.7042044

[22] S. R. Arya and B. Singh, "Performance of DSTATCOM Using Leaky LMS Control Algorithm," in IEEE Journal of Emerging and Selected Topics in Power Electronics, vol. 1, no. 2, pp. 104-113, June 2013. doi: 10.1109/JESTPE.2013.2266372

[23] M. Badoni, A. Singh and B. Singh, "Comparative Performance of Wiener Filter and Adaptive Least Mean Square-Based Control for Power Quality

Improvement," in IEEE Transactions on Industrial Electronics, vol. 63, no. 5, pp. 3028-3037, May 2016. doi: 10.1109/TIE.2016.2515558.

[24] J. B. Evans, P. Xue and B. Liu, "Analysis and implementation of variable step size adaptive algorithms," in IEEE Transactions on Signal Processing, vol. 41, no. 8, pp. 2517-2535, Aug 1993. doi: 10.1109/78.229885.

[25] J. F. Liu, Z. Q. Jiang, J. Li and X. Huo, "A Novel Variable Step-Size LMS Adaptive Filtering Algorithm Based on Lorentzian Function," in Command Control and Simulation, vol. 31, issue. 2, pp. 42-44, 2009.

[26] M. Badoni, A. Singh and B. Singh, "Variable Forgetting Factor Recursive Least Square Control Algorithm for DSTATCOM," in IEEE Transactions on Power Delivery, vol. 30, no. 5, pp. 2353-2361, Oct. 2015. doi: 10.1109/TPWRD.2015.2422139.

[27] M. O. Sayin, N. D. Vanli and S. S. Kozat, "A Novel Family of Adaptive Filtering Algorithms Based on the Logarithmic Cost," in IEEE Transactions on Signal Processing, vol. 62, no. 17, pp. 4411-4424, Sept.1, 2014, doi: 10.1109/TSP.2014.2333559.

[28] Huang, Fuyi & Zhang, Jiashu & Zhang, Sheng. (2018). "A family of robust adaptive filtering algorithms based on sigmoid cost". Signal Processing. 149. 10.1016/j.sigpro.2018.03.013.

[29] C.S. Solanki, "Solar Photovoltaics: Fundamentals Technologies And Applications", Prentice-Hall Of India Pvt. Limited, 2009.

[30] M. Liserre, T. Sauter and J. Y. Hung, "Future Energy Systems: Integrating Renewable Energy Sources into the Smart Power Grid Through Industrial Electronics," in IEEE Industrial Electronics Magazine, vol. 4, no. 1, pp. 18-37, March 2010. doi: 10.1109/MIE.2010.935861.

[31] S. Kumar, A. K. Verma, I. Hussain, B. Singh and C. Jain, "Improved EPLL Based Control of Grid Interfaced Solar PV System under Variable Solar Intensity," IEEE Industry Applications Magazine, Early Access.

[32] B. Singh, M. Kandpal and I. Hussain, "Control of Grid Tied Smart PV-DSTATCOM System using an Adaptive Technique," IEEE Trans. Smart Grid, vol. 9, no. 5, pp. 3986-3993, Sept. 2018.

[33] K. Mathuria, I. Hussain, B. Singh and N. Kumar, "A Quadrature Oscillator-Based DT for Accurate Estimation of Fundamental Load Current for PV System in Distribution Network," in IEEE Transactions on Industrial Informatics, vol. 15, no. 6, pp. 3324-3333, June 2019, doi: 10.1109/TII.2018.2875028.

[34] M. B. Shadmand, M. Mosa, R. S. Balog and H. A. Rub, "An improved MPPT technique for high gain DC-DC converter using model predictive control for photovoltaic applications," 2014 IEEE Applied Power Electronics Conference and Exposition - APEC 2014, Fort Worth, TX, 2014, pp. 2993-2999. doi: 10.1109/APEC.2014.6803730.

[35] M. W. Rahman, C. Bathina, V. Karthikeyan and R. Prasanth, "Comparative analysis of developed incremental conductance (IC) and perturb & observe (P&O) MPPT algorithm for photovoltaic applications," in Proc. 10th International Conference on Intelligent Systems and Control (ISCO), Coimbatore, 2016, pp. 1-6.

[36] M. Killi and S. Samanta, "Modified Perturb and Observe MPPT Algorithm for Drift Avoidance in Photovoltaic Systems," IEEE Trans. Industrial Electronics, vol. 62, no. 9, pp. 5549-5559, Sept. 2015.

[37] M. A. Elgendy, B. Zahawi and D. J. Atkinson, "Evaluation of incremental conductance MPPT algorithm at low perturbation rates," in Proc. 7th IET International Conference on Power Electronics, Machines and Drives (PEMD 2014), Manchester, 2014, pp. 1-6.

[38] J. W. Kimball and P. T. Krein, "Discrete-Time Ripple Correlation Control for Maximum Power Point Tracking," IEEE Trans. Power Electronics, vol. 23, no. 5, pp. 2353-2362, Sept. 2008.

[39] D. C. Huynh, T. N. Nguyen, M. W. Dunnigan and M. A. Mueller, "Dynamic particle swarm optimization algorithm based maximum power point tracking of solar photovoltaic panels," in Proc. IEEE Inter. Sympm. on Industrial Electronics, Taipei, Taiwan, 2013, pp.1-6.

[40] M. Das and V. Agarwal, "Novel High-Performance Stand-Alone Solar PV System With High-Gain High-Efficiency DC–DC Converter Power Stages," IEEE Trans. Industry Applications, vol. 51, no. 6, pp. 4718- 4728, Nov.-Dec. 2015.

LIST OF PUBLICATIONS

1. Neeraj Singh Bisht, Ankita Arora, “Comparison of Adaline and Sigmoid based adaptive Least Mean Square algorithms for control of Shunt Active Power Filter”, 2022 IEEE Delhi Section Conference (DELCON), 2022, pp. 1-6, doi: 10.1109/DELCON54057.2022.9753533.

2. Neeraj Singh Bisht, Ankita Arora, “Control of DSTATCOM using Sigmoidal Cost based Logarithmic Algorithms in Grid Connected Distribution Systems”, 2022 International Conference on Electronics and Renewable Systems (ICEARS), 2022, pp. 260-265, doi: 10.1109/ICEARS53579.2022.9752434.

3. Neeraj Singh Bisht, Ankita Arora, “Control of PV Based DSTATCOM Using Adaptive Sigmoidal Least Absolute Difference and Least Mean Fourth Algorithms”, 2022 International Conference on Distributed Computing and Electrical Circuits and Electronics (ICDCECE) ,2022.